

1
2 **Lithospheric mantle evolution monitored by overlapping large igneous**
3 **provinces: case study in southern Africa.**
4

5
6 **F. Jourdan^{a*}, H. Bertrand^b, G. Féraud^c, B. Le Gall^d, M.K. Watkeys^e**
7

8
9 *^aWestern Australian Argon Isotope Facility, Department of Applied Geology & JdL-CMS,*
10 *Curtin university of Technology, GPO Box U1987, Perth, WA 6845; Australia.*

11 *^bUMR-CNRS 5570, Ecole Normale Supérieure de Lyon et Université Lyon 1, 69364 Lyon,*
12 *France*

13 *^cUMR-CNRS 6526 Géosciences Azur, Université de Nice-Sophia Antipolis, 06108 Nice,*
14 *France*

15 *^dUMR-CNRS 6538, Institut Universitaire Européen de la Mer, 29280, Plouzané, France,*

16 *^eSchool of Geological and Computer sciences, University of Natal. Republic of South Africa*
17

18 * f.jourdan@curtin.edu.au
19

20 *Keywords : Large igneous province ; lithospheric mantle, mantle sources, Umkondo, Karoo,*
21 *mantle plume.*
22

23 **Abstract**
24

25 Most of the studies on the large igneous provinces (LIPs) focus on Phanerozoic times and in
26 particular those related to the disruption of Pangea (e.g. CAMP, Karoo, Parana-Etendeka,) while Precambrian LIPs (e.g. Ventersdorp, Fortescue) remain less studied. Although the
27 investigation of Precambrian CFBs is difficult because of their poorly preserved character, assessing their chemical composition in parallel with younger overlapping LIP is fundamental
28 for monitoring the evolution of the mantle composition through time.
29

30
31 Recent ⁴⁰Ar/³⁹Ar dating of the Okavango giant dyke swarm (and related sills) showed that ~
32 90% of the dykes were emplaced at 179 ± 1 Ma and belong to the Karoo large igneous

33 province whereas ~10% of dykes yielded Proterozoic ages (~1-1.1 Ga). Here, we provide
34 new major, trace and Rare Earth element analyses of the low-Ti Proterozoic Okavango dyke
35 swarm (PODS) that suggest, combined with age data, a cognate origin with the 1.1 Ga
36 Umkondo large igneous province (UIP).

37 The geochemical characteristics of the PODS and UIP basalts are comparable to those of
38 overlapping low-Ti Karoo basalts and suggest that both LIPs were derived from similar
39 enriched mantle sources. A mantle plume origin for these LIPs is not easily reconciled with
40 the chemical dataset and the coincidence of two compositionally similar mantle plume acting
41 900 Myr apart is unlikely. Rather, we propose that the Umkondo and Karoo large igneous
42 provinces monitored the slight evolution of a shallow enriched lithospheric mantle from
43 Proterozoic to Jurassic.

44

45 *Keywords:* Large igneous provinces, Continental flood basalts, Lithospheric mantle,
46 Umkondo, Karoo, Geochemistry.

47

48 **1. Introduction**

49

50 The Continental Flood Basalts (CFB) consist of large volume of magma (on the order of
51 several million km³) emplaced over a relatively brief time span. Whereas most of the studies
52 focus on the Phanerozoic CFBs and particularly those related to the Pangea disruption (e.g.
53 CAMP, Karoo-Ferrar, Parana-Etendeka, Deccan; see for instance [Hawkesworth et al., 1999](#)
54 and [Courtillot and Renne, 2003](#)), Precambrian CFBs such as Ventersdorp, Fortescue,
55 Umkondo ([Eriksson, 2002](#); [Ernst and Buchan, 2003](#)) remain less studied. Precambrian CFBs
56 are frequently highly deformed and eroded and are mostly represented by dykes, sills, layered
57 intrusions and more rarely minor remnants of flood basalts ([Ernst and Buchan, 2003](#)).
58 Although the investigation of Precambrian CFBs is hindered by their poorly preserved
59 character, their study is fundamental for monitoring the evolution of the mantle composition
60 through time. This is particularly relevant when old CFB are spatially overlapped by younger
61 ones ([Iacumin et al., 2003](#)).

62 Recent geochronological studies of the Okavango giant dyke swarm ([Le Gall et al., 2005](#))
63 (and related sill satellites) showed that ~ 88% of the dykes were emplaced at 179 ± 1 Ma (n=
64 14; [Le Gall et al., 2002](#), [Jourdan et al., 2004](#), [Jourdan et al., 2005](#)) and belong to the Karoo
65 large igneous province. However, it has also been demonstrated that the swarm includes ~

66 10% of Proterozoic dykes (Jourdan et al., 2004). The latter yielded a wide range of imprecise
67 $^{40}\text{Ar}/^{39}\text{Ar}$ “speedy step-heating” (2-3 heating steps on few plagioclase minerals used only to
68 discriminate Jurassic and Precambrian dykes; Jourdan et al., 2004) ages ranging from 850 to
69 1700 Ma. One plateau age (959 ± 5 Ma) and one weighted-mean age (983 ± 4 Ma), both
70 possibly suffering of some Ar perturbation, approximate the emplacement age of the swarm.
71 In addition, geochemistry was used as a discriminant tool between Jurassic and Proterozoic
72 populations. Whereas Karoo dykes were shown to be exclusively high-Ti tholeiites ($\text{TiO}_2 > 2$
73 wt.%, the Proterozoic Okavango dyke swarm and related sills (PODS hereafter) consist only
74 of low TiO_2 (< 2 wt.%) tholeiites. The latter are compositionally similar to the Karoo low-Ti
75 basaltic sub-province that represents the prevailing volume of the Karoo LIP (Jourdan et al.,
76 2007). The purpose of the initial study was to demonstrate that the Jurassic dyke swarm was
77 emplaced following a reactivated direction, and does not represent a Jurassic pristine structure
78 (Jourdan et al., 2004). However, poor consideration was addressed to the Proterozoic dykes
79 and their geodynamic significance. Here, we provide new major, trace and rare earth elements
80 analyses of the Precambrian dykes. We will discuss two hypotheses for the PODS origin: (1)
81 it is part of the recently discovered 1.1 Ga Umkondo igneous province (UIP, Hanson et al.,
82 1998) or (2) it belongs to a Kibaran post-orogenic rifting. In a second part, we compare the
83 composition of the PODS and the low-Ti Karoo Jurassic magmatism in order to monitor the
84 evolution of the underlying mantle through time.

85

86 **2. Geological setting and samples descriptions**

87

88 The N110°-trending giant Okavango dyke swarm and related sills intrude mainly Archaean
89 (Zimbabwe craton) and Proterozoic (e.g. the Magondi belt) rocks and the metamorphic
90 Limpopo-Shashe belt (Le Gall et al., 2002). The swarm is crosscut at high angle by the ~100
91 km long dry Shashe River, allowing efficient sampling. From the 77 rocks sampled along the
92 Shashe River and surroundings, 11 were assigned to the Proterozoic, based on their speedy
93 step-heating ages and major element composition (Jourdan et al., 2004). Eight dykes and 2
94 sills were sampled along the Shashe River and 1 sill (Bot0003) comes from further south of
95 the swarm (Fig. 1).

96 Whereas the dimension of the Jurassic dyke swarm is relatively well constrained by
97 aeromagnetic survey (~1500 x 100 km; Reeves et al., 2000; Chavez Gomez, 2001), the
98 extension of the Proterozoic swarm remains unknown, because it is virtually impossible to

99 differentiate between the two swarms by aero-magnetic measurements (Tshoso et al., 2002;
100 Aubourg et al., 2008). Along the Shashe river (the only section allowing a systematic
101 sampling across the dyke swarm), $^{40}\text{Ar}/^{39}\text{Ar}$ dating coupled with geochemistry (Jourdan et al.,
102 2004) show that Proterozoic dykes represent ~10 % of the ODS and are mostly restricted
103 within a 20 km-wide corridor located in the center of the ODS (Fig. 1b-c). The Proterozoic
104 dykes inside the Shashe River vary in thickness from 4 to 20 m. The three sills investigated
105 consist of small elongated and rounded sheets of dolerites located in the Shashe River (Bot11
106 and Bot01) and in eastern Botswana (Bot0003; Fig. 1b,c).

107 The Proterozoic dykes and sills consist of fine to medium grained olivine-free dolerites with
108 an ophitic to sub-ophitic texture. They contain mostly plagioclase and pyroxene (augite and
109 pigeonite) with minor Ti-magnetite and pyrite. Amphibole occurs in almost all samples
110 (except the two sills Bot11 and Bot0003) as replacement of the pyroxene, suggesting the
111 occurrence of a weak low-grade greenschist metamorphism. Amphibole is sometimes
112 accompanied by minor biotite. The alteration phases are mostly chlorite and sericite. The
113 modal composition of the Proterozoic dykes is not easily distinguishable from that of the
114 Jurassic dykes of the Okavango swarm. The most reliable discriminant seems to be amphibole
115 which is not observed in Karoo dolerites except in rare more differentiated samples (Jourdan
116 et al., 2004). However, the existence of Proterozoic amphibole-free rocks makes this criteria
117 somewhat misleading.

118

119 **3. Geochemistry**

120

121 The eleven Proterozoic samples were analyzed for major, trace and rare earth (REE)
122 elements (Table 1). They were crushed and powdered in an agate miller. Major and trace
123 elements were determined on fused disc and pressed powder pellets, respectively and were
124 analyzed by XRF (Philips PW 1404 spectrometer) at University of Lyon. REE, U and Th
125 were measured at the Chemex University (Canada). Analytical uncertainties vary from 1% to
126 2% and from 10% to 20% for major and trace elements respectively, depending on the
127 concentration of the element.

128 The eight dykes and three Proterozoic sills have low TiO_2 (0.5-2.1 wt.%) and low P_2O_5
129 (0.03-0.23 wt.%) contents (Fig. 2). They are quartz- or olivine-normative tholeiites. SiO_2 and
130 alkali contents range from 48.9 to 54.3 wt.% and from 2.3 to 4 wt.%, respectively. They are
131 classified as basalts and basaltic-andesites in the TAS diagram (Le Bas et al., 1986; not

132 shown). MgO and Mg# [$100 \times \text{Mg}/(\text{Mg}+\text{Fe}^{2+})$, considering $\text{Fe}_2\text{O}_3/\text{FeO} = 0.15$] vary from 3.9
133 to 8.2 wt.% and from 34 to 63, respectively, indicating the moderately evolved character of
134 the rocks (Fig. 2). Mg# exhibits a negative co-variation with SiO_2 , Na_2O and TiO_2 , and a
135 positive co-variation with CaO and Al_2O_3 (Fig. 2). These trends suggest that dolerites have
136 been affected by differentiation processes involving fractional crystallization. The Proterozoic
137 rocks can be subdivided into two sub-groups: (i) a group including 3 samples with relatively
138 moderate TiO_2 and SiO_2 contents (≥ 1.7 wt.% TiO_2 and ≤ 52.1 wt.% SiO_2) and with a low
139 Mg# (≤ 47), and (ii) a group of 8 samples with lower TiO_2 and higher SiO_2 contents (≤ 1 wt.%
140 TiO_2 and ≥ 52.5 wt.% SiO_2 ; Fig. 2) and with a Mg# > 47 . Hereafter these two groups are
141 referred to as the high- and low-Mg# groups, respectively. The low-Mg# sub-group includes
142 two sills (Bot01 and Bot11) and one dyke (Bot15) from the Shashe River and thus the
143 difference between the two groups cannot be related to the nature of the intrusion (i.e. sill or
144 dyke). Moreover, it is unlikely that the chemical difference between the groups was produced
145 by different degrees of alteration as the discriminant elements do not co-vary with LOI
146 contents which are relatively low in the two groups (0.5 to 1.4 wt.%).

147 The two sub-groups mentioned above display distinct trends on most trace elements plots
148 (Fig.3). The amount of incompatible (e.g. Rb, Y) and compatible (e.g. Cr) trace elements
149 increases and decreases, respectively, as Mg# decreases, in accordance with fractional
150 crystallization within each sub-group. The PODS have low Ce/Pb values (from 0.5 to 5.8),
151 largely lower than the accepted values for OIB and MORB (~ 25 ; Chauvel et al., 1995) and
152 plots in the field of subduction-related rocks.

153 On the multi-elements normalized diagrams, the Proterozoic dolerites show a moderate
154 enrichment in the most incompatible trace elements (ITE; $\text{Rb}/\text{Y}_n = 6-34$ Fig. 4). The patterns
155 are characterized by negative anomalies for Nb ($\text{Nb}/\text{Nb}^* = 0.18-0.43$), Sr ($\text{Sr}/\text{Sr}^* = 0.28-$
156 0.71), P ($\text{P}/\text{P}^* = 0.53$ to 0.79) and Ti ($\text{Ti}/\text{Ti}^* = 0.54$ to 0.90) which are more pronounced for
157 the high-Mg# sub-group. The REE patterns (Fig.5) show a relatively slight Light REE
158 (LREE) enrichment compared to Heavy REE (HREE; $\text{La}/\text{Yb}_n = 3.3-4.4$) and a poor HREE
159 fractionation ($\text{Sm}/\text{Yb}_n = 1.5-1.7$). A slight negative anomaly in Eu ($\text{Eu}/\text{Eu}^* = 0.70-0.92$)
160 concurs with the Sr anomaly as an indication of plagioclase fractionation.

161 The dyke compositions display no chemical variation across the width of the swarm. The
162 sills have indistinguishable composition compared to the dykes.

163

164 **4. Discussion**

165

166 *4.1. Petrogenesis of the PODS*

167

168 4.1.1. Partial melting

169

170 Equilibrium non-modal melting has been modeled by using the standard equation of [Shaw](#)
171 [\(1967\)](#). In order to explain the poor fractionation of the Middle REE (MREE) and HREE, we
172 used a garnet-free, spinel bearing lherzolite (< 80 km depth) with the same modal
173 composition as used by [Jourdan et al. \(2007\)](#) for the Karoo low-Ti basalts (55% olivine, 15%
174 orthopyroxene, 28% clinopyroxene and 2% spinel). A slightly more enriched source
175 composition has been chosen to account for the small difference between PODS and Karoo
176 rocks ($\text{La/Yb}_{\text{source}}=3.27$ and 2, respectively). Partition coefficients are from [McKenzie and](#)
177 [O’Nions \(1991\)](#). We reported the melting curves in the $(\text{La/Yb})_n$ vs. $(\text{Eu/Yb})_n$ and $(\text{Sm/Yb})_n$
178 vs. $(\text{La/Sm})_n$ plots ([Fig. 6](#)). The calculated melts, produced in the range of 5-10% melting,
179 adequately match the observed REE variations. The low-Mg# group requires a higher melting
180 rate (9-10 %) compared to the high-Mg# group (5-8%), in order to fit the lower $(\text{La/Sm})_n$
181 values of the former group.

182

183 4.1.2. Fractional crystallization

184

185 Petrographic observations and major and REE element behavior show that the PODS rocks
186 cannot be considered as primary mantle melts and that they underwent fractional
187 crystallization of gabbroic assemblages. MELTS algorithm ([Ghiorso and Sack, 1995](#); [Smith](#)
188 [and Asimow, 2005](#)) calculates the liquid lines of descent of magmas and provides the
189 composition of both residual liquids and cumulate minerals. We carried out isobaric runs
190 using various pressures ($P=0.5-5$ Kbars) and H_2O contents ($\text{H}_2\text{O}=0-2$ wt. %) conditions (e.g.
191 [Fig. 7](#)) and $f\text{O}_2=\text{QFM}$ (quartz-fayalite-magnetite). We used one of the less differentiated
192 sample as starting composition (Bot0003; $\text{Mg\#} = 66$). The homogeneous composition of the
193 PODS hinders the best estimate of the run conditions, yet the fractional crystallization at low
194 pressure (1-2 Kbars) under anhydrous conditions satisfactorily fits the high-Mg# group. The
195 amount of fractionation (up to ~80 %) of a gabbroic assemblage (clinopyroxene +
196 plagioclase) seems however too high to be realistic, ruling out that the data spread can be

197 explained by fractional crystallization alone. The low-Mg# group shows much more
198 dispersion of the sample compositions but does not include enough samples (n=3) to allow
199 fractional crystallization modeling. In any case, this group requires different source starting
200 conditions (higher degree of partial melting (Fig. 6) or different source composition?) to be
201 accounted for.

202 Minor variations within the data set not accounted for by differentiation processes could be
203 best explained by the contribution of (1) small crustal contamination, but this is hard to verify
204 in absence of isotope data and/or (2) weak hydrothermal alteration (if present) that may have
205 happened during the low grade metamorphism phase. In addition, the starting composition
206 assumed in this model is not a primary magma and does not take into account earlier
207 fractionating assemblages which can explain substantial differences among the samples if
208 several magma chambers are involved.

209 In summary, a combination of partial melting of a common mantle source and subsequent
210 fractionation processes may account for most of the variations of the PODS samples.
211 However, minor alteration, crustal contamination or mantle source heterogeneity (or any
212 combination of the three) seems also to be required to account for some of the observed
213 discrepancies.

214

215 *4.2. Mantle source of the PODS*

216

217 The geochemical characteristics of the low-Ti PODS are similar to those reported for low-Ti
218 Phanerozoic CFB (e.g. Karoo-Ferrar, CAMP, Parana-Etendeka). For instance, the rocks are
219 enriched in ITE and in LREE relatively to HREE and display a strong Nb anomaly. The
220 mantle sources at the origin of CFBs are yet not well resolved with models ranging from
221 mantle plume head (Morgan, 1981; White and McKenzie, 1989; Campbell and Griffiths,
222 1990; Hill, 1991; Wilson, 1997, Courtillot et al., 1999) to the sub-continental lithospheric
223 mantle (SCLM; Hawkesworth et al., 1984, 1999; Bertrand, 1991; Molzahn and Reisberg
224 1996; Jourdan et al., 2003, 2007) or perispheric mantle (Anderson et al., 1992, 1994). Some
225 authors have suggested that each CFB is more or less distinctive and that the origin of these
226 provinces cannot be explained by a unique “dogmatic” model (e.g. Hawkesworth et al., 1999;
227 Jourdan et al., 2007). For instance, the Deccan (Peng et Mahoney, 1995) or Ethiopia-Yemen
228 (Pick et al., 1999) traps fit particularly well the deep mantle plume model as suggested by
229 their OIB-like elemental and isotopic geochemistry, whereas the Karoo mantle sources are

230 more likely located either partially or totally in the SCLM (e.g. [Sweeney et al., 1994](#);
231 [Molzahn and Reisberg., 1996](#); [Jourdan et al., 2007](#)).

232 The La/Nb-La/Ba plot is commonly used to investigate the origin of CFB rocks ([Fig. 8](#),
233 [Saunders et al., 1992](#); [Hawkesworth et al., 1999](#), [Nomade et al., 2002](#), [Jourdan et al., 2007](#))
234 and is particularly relevant when isotopic analyses are not available. Positive correlations
235 between La/Nb and La/Ba reflect OIB and/or asthenospheric mantle source(s) whereas
236 negative correlations are diagnostic of a strong lithospheric contribution. These ratios are
237 almost not modified by petrogenetic processes ([Hawkesworth et al., 1999](#)) and thus, likely
238 represent mantle source signature(s). The PODS rocks display a similar mantle trend as the
239 Karoo magmas ([Jourdan et al., 2007](#)), though with a shallower slope. Both groups point
240 toward relatively low La/Ba and high La/Nb values. Following [Saunders et al. \(1992\)](#), we
241 interpret these values as indicating a strong contribution from the SCLM. Similarly, the Zr/Y-
242 Ti/Y plot ([Fig. 9](#)) shows that the PODS rocks are clustered between the bulk earth
243 composition and a “post-Archaean shale” component. This pole has been commonly
244 interpreted as representing a subducted sediment signature ([Brewer et al., 1992 and references](#)
245 [inside](#)) possibly located in the SCLM. Two samples align themselves on the primitive
246 mantle/MORB – OIB array, in direction of the OIB field. This might be interpreted as a
247 potential evidence of a small contribution of a lamproitic or a mantle plume component in the
248 genesis of these two rocks, but the evidences are tenuous.

249 As mentioned above, the Ce/Pb (0.5-5.8; [Fig. 3](#)) is by far too low to reflect OIB or MORB
250 mantle (Ce/Pb>20; e.g. [Chauvel et al., 1995](#)) and is closer in composition to subduction-
251 related magmas (Ce/Pb<10). Although the PODS do not display calc-alkaline characteristics,
252 fluids released from a previous subduction may have “polluted” the SCLM ([Hawkesworth et](#)
253 [al., 1999](#)). Concerning the two PODS sub-groups (i.e. low- and high-Mg#), their similarities
254 in ITE and REE patterns and concentrations, and their behavior in discriminant diagrams
255 strongly suggest that they are issued from a similar mantle source. The difference between the
256 two groups is mostly expressed by P, Ti and Nb anomaly. However, these anomalies are
257 neither correlated with the Mg# nor with the LREE/HREE variations (not shown), suggesting
258 that these differences are not due to fractionation or melting processes. Therefore, we suggest
259 that these differences might be induced by small scale heterogeneities of a common mantle
260 source.

261 In summary, the PODS rocks are hardly assigned to an OIB-like asthenospheric or
262 mesospheric mantle source model (i.e. mantle plume; [Campbell and Griffiths, 1990](#)) neither
263 to a calc-alkaline subduction-related magmatism (despite common features as low Ce/Pb and

264 Nb anomaly). The best source candidate suggested by our data is therefore likely to be located
265 in the lithospheric mantle ($\text{La/Nb} > 2$) metasomatically enriched by a previous subduction
266 event ($\text{Zr/Y} \sim 6-7$, $\text{Ce/Pb} < 10$). A 1.4-1.3 Ga subduction event (Kibaran subduction) has been
267 reported in the Namaqua orogenic belt (Kampunzu et al., 2000 and references therein) and
268 was suspected to have been responsible for the enriched signature of the 1.1 Ga Kwebe
269 within plate volcanism (Fig. 10; Kampunzu et al., 2000). We speculate that the Kibaran
270 subduction may have been also responsible for the PODS and related sills mantle source
271 enrichment. Crucial isotopic analyses would be required for assessing this hypothesis.

272

273 4.3. Geodynamic setting of the PODS?

274

275 4.3.1. Age of the PODS

276

277 The PODS samples yielded “speedy step-heating” ages ranging from 850 to 1700 Ma
278 (Jourdan et al., 2004). This age range does not reflect an extremely long-lasting geological
279 process but is induced by the poor constraints inherent to the speedy step-heating method
280 which cannot resolve the complex interaction between alteration and excess of Ar (Jourdan et
281 al., 2004). A plateau and a weighted-mean ages of 983 ± 4 (sample Bot0083) and 959 ± 5 Ma
282 (sample Bot0003) were obtained on plagioclase-separates using standard step-heating method
283 (Jourdan et al., 2004).

284 The younger sample has a flat $^{37}\text{Ar}_{\text{Ca}}/^{39}\text{Ar}_{\text{K}}$ spectrum, apparently indicative of a negligible
285 alteration. On the other hand, the older sample shows a strongly tilde-shaped $^{37}\text{Ar}_{\text{Ca}}/^{39}\text{Ar}_{\text{K}}$
286 that can be attributed either to important alteration (Verati and Féraud, 2003) or to strong
287 mineral zoning. When plagioclase has been altered into a significant amount of sericite (i.e. >
288 20 %), this can produce statistically valid but spuriously young “alteration” plateau ages due
289 to the large K content of sericite ($\text{K}_2\text{O} \sim 10$ wt.%) compared to plagioclase (~ 0.05 wt.%). In
290 any case, it is not clear whether these ages represent crystallization ages or a partial/total reset
291 of the isotopic system by a subsequent low-degree metamorphism (as evidenced by
292 amphibolitisation of the pyroxene phenocrysts).

293 For comparison, $^{40}\text{Ar}/^{39}\text{Ar}$, K/Ar and Rb/Sr ages obtained so far on the basic Mesoproterozoic
294 CFB-related rocks from southern-Africa/Antarctica (Umkondo large igneous province (UIP);
295 Fig. 10) appear to be strongly perturbed with ages ranging from 600 ± 24 to 1802 ± 100 Ma
296 (Kruger et al., 2000; Key and Ayers, 2000; Reimold et al., 2000; Burger and Valreven, 1979
297 and 1980). In contrast, robust zircon and baddeleyite U/Pb TIMS ages obtained on the same

298 formations (plus additional rocks from different localities) are restricted between 1106.1 ± 2.0
299 and 1112.0 ± 0.5 Ma (Shwartz et al., 1996; Hanson et al, 1998, 2004, 2006; Singletary et al.,
300 2003). This suggests that rocks emplaced during the Mesoproterozoic period suffered strong
301 perturbations that so far preclude the use of the K/Ar, Rb/Sr and even $^{40}\text{Ar}/^{39}\text{Ar}$
302 geochronometers for investigating their crystallization ages.
303 In absence of further evidence on the meaning of the $^{40}\text{Ar}/^{39}\text{Ar}$ ages obtained in Jourdan et al.
304 (2004), we could propose two different hypotheses; (1) these ages reflect
305 alteration/metamorphism processes with strong perturbation of the $^{40}\text{Ar}/^{39}\text{Ar}$ chronometer and
306 thus the magmatism is likely to be substantially older (possibly as old as and belonging to the
307 1.1 Ga Umkondo magmatism; Hanson et al., 1998 and 2004), or (2) these dates are true
308 crystallization ages and are possibly representative of a distention process associated to the
309 late-Kibaran orogeny (1.0 Ga), In the following parts, we test these two hypotheses.

310

311 *4.3.2. Post-Kibaran failed rift dykes hypothesis*

312

313 The “Kibaran” Mesoproterozoic belt stretches over 3000 km long through central and
314 southern Africa. The Kibaran belt is a broad patchwork of smaller similarly aged belts. It is
315 located along the eastern and southern part of the Congo craton (Fig. 10; Kampunzu et al.,
316 1998; Kokonyangi et al., 2004). Between 1.4 and 1.0 Ga, Kibaran metasedimentary and
317 igneous rocks were involved in two compression events (Johnson and Oliver, 2000) that
318 cannot be truly dissociated into 2 distinct orogens (Kampunzu et al., 1998). The Kibaran
319 orogeny includes an active continental margin (Kibaran orogeny sensu stricto, 1.4-1.2 Ga)
320 followed by a continental collision (Namaquan orogeny; 1.1-1.0 Ga). The late stage of the
321 Namaquan orogeny was marked by numerous granitic intrusions, which yielded Rb-Sr
322 isochron ages ranging from 966 ± 21 to 1006 ± 44 Ma (Cahen and Ledant, 1979; Cahen et al,
323 1984; Ikingura et al. ,1990) and U/Pb ages on zircon separate at 1.02-1.0 Ga (Singletary et al.,
324 2003). Very few examples of major dyke swarm emplaced in compressive environments
325 exist. Féraud et al. (1987) identified alkaline dykes linked with the Indo-European, African
326 and Arabian plate collision. These dykes are narrow (0.5 to few meters wide) and follow the
327 direction of the maximum horizontal compressive stress. Another example is given by the
328 ~700 km- long Independence dyke swarm, occurring throughout southeastern California in
329 relation to the subduction of the Farallon plate beneath the North American plate (Chen and
330 Moore, 1979; Coleman et al., 2000). The Independence swarm shows a typical bimodal arc-
331 magmatism-type composition (e.g. Coleman et al., 2000; Jourdan et al., 2005) and is

332 emplaced perpendicular to the direction of the subducting plate and to the main compressive
333 stress vector.

334 The PODS is roughly located at high-angle to the Kibaran belt, following its maximum
335 compressive vector, and could therefore represent a direct expression of the Kibaran orogeny.
336 However, two points argue against this hypothesis: (1) the PODS dykes are substantially
337 thicker than those mentioned in pure collisional settings (Féraud et al., 1987), (2) they do not
338 exhibit an alkaline or a calc-alkaline composition as expected in a compressive system, but a
339 typical CFB composition not commonly reported in an orogenic context.

340

341 4.3.3. Comparison between PODS and the Umkondo igneous province

342

343 Recent paleomagnetic and geochronological (mainly zircon U/Pb analyses) investigations
344 suggest a common origin to Proterozoic tholeiites occurring throughout the southern Africa
345 and possibly Antarctica (Fig. 10; Hanson et al., 2004). These terms are regrouped as the
346 Umkondo igneous province (UIP), given from the name of Umkondo Zimbabwe dolerite
347 formation of the same age. The UIP is now defined as a widespread Mesoproterozoic
348 continental flood basalt emplaced in southern Africa and Antarctica (Hanson et al., 1998 and
349 2004). It consists of tholeiitic mafic intrusions (sills and dyke swarms) and scarce remnants
350 of eroded basaltic lava-flows emplaced over an estimated paleo-surface of $\sim 2.5 \cdot 10^6$ km² (Fig.
351 10). This igneous event is contemporaneous but not directly related to the collision of the
352 Laurentia and Kalahari cratons (Grenville-Llano and Namaqua-Natal Orogeny) which
353 contributed to the formation of the Rodinia mega-continent (Hanson et al., 1998; Dalziel et
354 al., 2000).

355 Robust ages clustered around 1.1 Ga have been obtained using zircon and baddeleyite U/Pb
356 TIMS technique (Hanson et al., 1998 and 2004). Unfortunately, contrary to geochronological
357 data, complete sets of major, trace and rare earth elements are still scarce and restricted to few
358 outcrops. We therefore compare the PODS only to the 1105 ± 2 Ma Zimbabwe Umkondo
359 dolerites (eastern Zimbabwe; Munyaniwa, 1999), the geochemically-related Guruve and
360 Mutare dykes (Northern Zimbabwe; Ward et al., 2000), although several generations of dykes
361 might be involved in this swarm (Hanson et al., 2006) and the 1108.6 ± 1.2 Ma Anna rust's
362 sheet (South Africa; Reimold et al., 2000 and references herein) (Fig. 10). The bimodal
363 (acidic and basic) sequence from Kwebe (western Botswana) yielded U-Pb zircon ages of
364 1106 ± 2 Ma and 1104 ± 16 Ma (Schwartz et al., 1996) but these rocks are not considered

365 here because their chemical composition present a large scatter due to alteration and
366 greenschist metamorphism (Kampunzu et al., 1998) .

367 The UIP dolerites are mostly low-Ti basaltic rocks ($\text{TiO}_2 = 0.4\text{-}1.9$ wt.%; except two high-Ti
368 samples) and are moderately evolved rocks with SiO_2 and Mg# mainly ranging from 48.8 to
369 57.0 wt.% and from 45 to 63, respectively. They show a moderate ITE enrichment ($\text{Rb}/\text{Y}_n =$
370 3.0-33.1) and a variable negative Nb anomaly (33 samples range from 0.12 to 0.95). Five
371 rocks from Kwebe (Kampunzu et al., 1998), 1 dyke from Mutare (Ward et al., 2000) and 1
372 dolerite from Zimbabwe (Munyaniwa, 1999) exhibit a positive Nb anomaly ranging from 1.14
373 to 2.28. However, it is not clear if the positive Nb anomaly feature is pristine or if it is due to
374 secondary K loss (K is used to in this study to calculate the Nb anomaly) during the slight
375 greenschist metamorphism. UIP dolerites display moderate REE fractionation mainly
376 concerning light REE ($\text{La}/\text{Ybn} = 1.7\text{-}7.7$; $\text{La}/\text{Sm}_n = 1.3$ to 4.3). Ce/Pb is low and varies from
377 1.6 to 7.3 for all the rocks. Compared to the PODS, the Umkondo dolerites share striking
378 similar characteristics. They display important overlap in major (Fig. 2) and trace (Fig. 3)
379 elements with for instance similar correlations between Mg# and TiO_2 , SiO_2 , Al_2O_3 and CaO
380 and between Zr and Y (not shown). Both groups show noticeable dominant Nb and Sr
381 anomaly and a low Ce/Pb ratio (<8). PODS and UIP are also characterized by a moderately
382 enriched ITE patterns (Fig. 4a, 4b) and REE (Fig. 5a, 5b) with unfractionated HREE. In the
383 Zr/Y-Ti/Y diagram (Fig. 9), most of the UIP and PODS rocks overlap pointing mainly toward
384 post Archaean shale component (except three outlier samples trending toward a high Ti/Y
385 component).

386 In order to compare the genesis of UIP and PODS rocks, the former were reported on the
387 melting modeling diagram (Fig.6). They strikingly plot on the same modeled curves as the
388 PODS and can be reproduced by a wider range (1.5 to 15 %) of melting of the same spinel
389 lherzolite source (Fig. 6). The only two high-Ti UIP dolerites identified so far, also match the
390 (2wt. %) garnet-bearing curve calculated by Jourdan et al. (2007) for the Karoo high-Ti
391 basalts.

392 The only significant difference between UIP and POD samples is shown by the Ba/Nb vs.
393 La/Nb plot (Fig. 8). The UIP rocks are subdivided into two groups showing different trends.
394 The Umkondo dolerites from Zimbabwe display the same negative trend as the PODS rocks,
395 pointing toward a lithospheric component whereas the Anna rust's sheet apparently follows a
396 positive (asthenospheric-like) correlation trend.

397 In summary, although the PODS might have been triggered by the intrusion of magma in
398 relation to the Kibaran compressional orogeny, it is more likely to be related to a CFB event

399 as monitored by its geochemical data. The only known CFB occurring at the end of the
400 Mesoproterozoic is the Umkondo magmatism. The Umkondo rocks share strikingly similar
401 composition with the PODS samples, thus arguing for the same mantle source. However, it is
402 still not clear if this mantle source has been tapped at two different periods or in a few Myr
403 time span. As the apparent ages obtained on PODS are possibly perturbed, the simplest
404 explanation would be that the PODS was emplaced contemporaneously to the UIP (1.1 Ga)
405 and may have a cognate magmatic origin. However, further dating based on robust zircon
406 and/or baddeleyite U/Pb analyses are required to test this hypothesis.

407

408 *4.4. Overlapping Umkondo and Karoo CFBs: a witness of SCLM evolution through time?*

409

410 The partial geographical overlap of Umkondo and Karoo CFBs (Fig. 1 and 10) provides a
411 good opportunity to test whether these two provinces share a similar mantle source or not. In
412 addition, the former case would allow to assess to what extent this common mantle source
413 may have evolved ~900 Myr apart, from 1.1 Ga to 180 Ma.

414 Since four decades, the Karoo magmatism was chemically investigated by various authors
415 (e.g. Cox, 1967; Hawkesworth et al., 1984; Sweeney et al., 1994; Jourdan et al., 2007). Data
416 gleaned through these studies show that the Karoo magmatism, as most of the CFBs, consists
417 of low- and high-Ti basalts (Cox, 1988). Although some authors have proposed a OIB-like
418 mantle plume origin for the Karoo magmatism (Ellam et al., 1992), a vast majority of workers
419 argue for a dominant contribution of a subduction-modified SCLM (e.g. Duncan et al., 1984;
420 Cox, 1988, Sweeney and Watkeys, 1990; Sweeney et al., 1994; Hawkesworth et al., 1999;
421 Elburg and Goldberg, 2000 Jourdan et al., 2007) with heat source provided by mechanisms
422 such as supercontinent shield effect (Coltice et al., 2007 and submitted)

423 Here, we compare the geochemistry of the Proterozoic UIP, exemplified by the low-Ti
424 PODS, to Jurassic low-Ti Karoo basalts from Botswana and Zimbabwe (Jourdan et al., 2007
425 and references inside). High-Ti rocks will not be considered here, as they are unknown in the
426 PODS, so far and are represented by only two samples in the UIP. These two CFB provinces
427 share many similar features. Both groups show a significant overlap concerning most of the
428 major (Fig. 2) and trace (Fig. 3) elements. They display similar enriched ITE patterns (Fig. 4).
429 All but seven (see discussion above) UIP samples bear a negative Nb anomaly ranging from
430 0.12 to 0.95 that compares to 0.22 to 0.81 for the low-Ti Karoo basalts. Both provinces have
431 REE patterns that show moderately fractionated LREE ($\text{La/Yb}_n = 2.0$ to 3.4 for Karoo low-Ti

432 basalts vs. 1.7-7.7 for UIP low-Ti basalts) but unfractionated mid-REE vs. HREE (Sm/Yb_n
433 from 1.2 to 1.6 for Karoo vs. 1.3-1.9 for UIP; Fig. 5).

434 However, significant differences distinguish the Proterozoic from the Jurassic basalts. In
435 general, PODS rocks have higher SiO₂ and ITE (e.g. Rb) contents and slightly lower contents
436 for other major and compatible elements (e.g. TiO₂ and Cr; Fig. 2, 3), for a given Mg#. The
437 most striking differences concern the ITE patterns, which display pronounced negative Sr, P
438 and Ti anomalies for the PODS basalts but not for the Karoo low-Ti basalts (Fig. 4). The UIP
439 also display more pronounced negative Nb anomalies as well as slightly lower Ce/Pb ratios in
440 average (Fig. 3). On the Zr/Y vs. Ti/Y diagram (Fig. 9) the trend toward the shale component
441 is more pronounced for the PODS than for Karoo low-Ti basalts. Globally, the PODS shows
442 stronger subduction characteristics than the Karoo basaltic rocks (e.g. Nb anomaly, Ce/Pb,
443 low Ti/Y and high La/Nb).

444 We further test if the Karoo and PODS low-Ti rocks have a similar mantle source by
445 comparing their batch melting model curves (Fig. 6). The Karoo trend is reproduced by 3 to
446 20 % melting of a slightly more depleted mantle source (La/Yb = 2 against 3.27 for UIP) and
447 using the same modal composition compared to the PODS (Jourdan et al., 2007). The two
448 curves are almost overlapping, strongly attesting for a similar, although not identical mantle
449 source for the two CFBs.

450 Therefore, the data suggest that the PODS and the Karoo low-Ti basaltic rocks originate
451 from enriched mantle sources that bear very close characteristics. These two magma suites
452 show strong and dominant SCLM mantle signatures (e.g. low Ce/Pb and important Nb
453 negative anomalies). Considering the 900 Myr interval between the two CFB events, the
454 differences observed between the Proterozoic and Jurassic rocks are tenuous. They can be
455 interpreted in term of (1) lateral and vertical heterogeneities in the SCLM, (2) evolution of the
456 SCLM from 1.1 Ga to 180 Ma or a combination of both. Consequently, hypothesis (2) would
457 imply that the (subduction-enriched?) SCLM underwent only a slight depletion since
458 Proterozoic times. Such depletion might be due to extraction of the widespread Umkondo
459 CFB. In that case, the enriched composition of the SCLM would be already established before
460 the 1.1 Ga Umkondo event. This proposition is strengthened as the Karoo rocks show a
461 noticeable decoupling between ²⁰⁶Pb/²⁰⁴Pb and ²⁰⁷Pb/²⁰⁴Pb which was interpreted by Jourdan
462 et al. (2007) as reflecting the contribution of a stable and old-enriched mantle source. As
463 mentioned above, and also proposed for Ferrar rocks from Droning Maud Land (Lutinen and
464 Furnes, 2000), the chemical enrichment of the source was suggested to represent a feature
465 inherited from a Proterozoic orogeny, possibly the 1.4-1.3 Ga Kibaran subduction (Kampunzu

466 [et al., 1998](#)). A similar approach has been conducted for the Late Archaean-Proterozoic (2.7
467 and 1.0 Ga) and Mesozoic (200 and 130 Ma) CFB magmatism in South America and
468 concluded also for only a slight evolution of the composition of the SCLM through time
469 ([Iacumin et al., 2003](#)).

470 These results have important bearing on the mantle plume issue at the origin of Umkondo
471 and Karro CFBs. As discussed above, no mantle plume signature is recognized in the PODS
472 and UIP dataset. Moreover the mantle plume hypothesis for both UIP and Karoo would
473 assume that two distinct plume heads sharing similar compositions would have been
474 emplaced 900 Myr apart, coming from laterally distinct source regions (considering the drift
475 of the African plate from 1.1Ma to 180Ma). It is unlikely that these requirements were
476 fulfilled, and we favor the persistence of a SCLM source slightly evolving through time.

477 Further work is required to monitor the evolution of the LIP mantle source through time in
478 southern Africa. This includes isotopic analysis on the PODS to highlight the similarities and
479 differences with the Karoo province, and investigation of Proterozoic and Archaean dykes of
480 other dykes swarms (e.g. Save-Limpopo, Olifant River and Palabora dyke swarms; [Jourdan et](#)
481 [al., 2006](#)).

482

483 **5. Conclusions**

484

485 The geochemical investigations on the mafic Proterozoic Okavango dyke swarm and related
486 sills (PODS) lead us to draw several conclusions:

487 (1) Geochemical characteristics (e.g. Nb anomaly, Ce/Pb ratio, ITE and REE pattern) suggest
488 that the PODS was derived from the melting of a shallow mantle source. This source is
489 different from the OIB or MORB mantle and is thought to represent sub-continental
490 lithospheric mantle (SCLM) enriched by fluids released during the 1.4-1.3 Ga Kibaran
491 subduction.

492 (2) The PODS shares similar geochemical characteristics with basaltic remnants scattered in
493 Botswana, Zimbabwe and South Africa and attributed to the 1.1 Ga Umkondo large igneous
494 province (UIP). Considering younger ~1 Ga disturbed Ar/Ar ages previously obtained, the
495 PODS is considered as either part of the UIP or issued from a UIP-like source reactivated
496 ~100 Myr later.

497 (3) The PODS and UIP CFB overlap and share similar characteristics with the 180 Ma low-Ti
498 Karoo CFB. Modeling suggests that both were derived from melting of a similar but not

499 identical enriched spinel-bearing mantle source. The resemblance between these Proterozoic
500 and Jurassic CFBs supports the tapping, 900 Ma apart, of a common enriched stabilized
501 SCLM attached to the African plate and is hard to reconcile with the melting of two distinct
502 mantle plumes. The slight depletion of the Karoo basalts relatively to the PODS suggests that
503 the extraction of the Umkondo magmas from the SCLM may have contributed to its relative
504 depletion. The southern African SCLM therefore inherited its characteristics since the
505 Mesoproterozoic and has probably undergone no major enrichment since this period.

506

507 **Acknowledgments**

508

509 This work is part of a partnership between the University of Botswana and the French
510 Universities of Nice, Lyon and Brest. We acknowledge the financial support of the CNRS (
511 grant INSU Intérieur de la Terre), the French Ministry of Foreign Affairs, the University of
512 Botswana (Grant RPC Kaapvaal Craton Project R#442), the SU-CRI 2E of the University of
513 Western Brittany and the Universities of Nice and Lyon. We are grateful to C. Tonani, Head
514 of the Cultural and Scientific Service of the French Embassy in Botswana for his support in
515 developing this program. M. Manetti and P. Capiez are thanked for analytical assistance. FJ
516 thanks E. Eroglu for discussion. Géosciences Azur contribution No. 433.

517

518 **References**

519

- 520 Anderson, D.L., Zhang, Y. S., Tanimoto, T., 1992. Plume heads, continental lithosphere,
521 flood basalts and tomography. In: B.C. Storey, Alabaster, T., Pankhurst, R.J. (Eds),
522 Magmatism and the Causes of Continental Break-up. Special Publication of the
523 Geological Society of London, pp. 99-124.
- 524 Anderson, D.L., 1994. The sublithospheric mantle as the source of continental flood basalts;
525 the case against the continental lithosphere and plume head reservoirs. *Earth and*
526 *Planetary Science Letters* 123, 269-280.
- 527 Aubourg, C., Tshoso, G., Le Gall, B., Bertrand, H., Tiercelin, J.-J., Kampunzu, A.B., Dymant,
528 J., Modisi M., 2008. Magma flow revealed by magnetic fabric in the Okavango giant dyke
529 swarm, Karoo igneous province, northern Botswana. *Journal of Volcanology and*
530 *Geothermal Research* 170, 247–261.

531 Bertrand, H., 1991. The Mesozoic tholeiitic provinces of northwest Africa: a volcano-tectonic
532 record of the early opening of Central Atlantic. In: A.B. Kampunzu, Lubala, R.T. (Eds),
533 Magmatism in extensional structural settings. The Phanerozoic African plate. Springer-
534 Verlag, Berlin Heidelberg, New York, pp. 147-188.

535 Boynton, W.V., 1984. Geochemistry of the rare earth elements: meteorite studies. In:
536 Henderson P. (Ed), Rare earth element geochemistry. Elsevier, pp. 63-114.

537 Brewer, T.S., Hergt, J.M., Hawkesworth, C.J., Rex, D and Storey, B.C., 1992. Coats Land
538 dolerites and the generation of Antarctic continental flood basalts. In: B.C. Storey,
539 Alabaster, T., Pankhurst R.J. (Editor), Magmatism and the causes of continental break up.
540 Geological Society Special Publication, pp. 185-208.

541 Burger, A.J., Walraven, F., 1979. Summary of age determinations carried out during the
542 period April 1977 to March 1978. South Africa Geological Survey Annals, 12: 209-218.

543 Burger, A.J., Walraven, F., 1980. Summary of age determinations carried out during the
544 period April 1978 to March 1979. South Africa Geological Survey Annals, 14: 109-118.

545 Cahen, L., Ledent, D., 1979. Précision sur l'age, la pétrogenèse et la position stratigraphique
546 des "granites à étain" de l'est de l'Afrique Centrale. Bulletin Société Belge Géologiques,
547 88: 33-49.

548 Cahen, L., Delhal, J., Vail, J.R., Bonhomme, M., Ledent, D., 1984. The geochronology and
549 evolution of equatorial Africa. Clarendon Press, Oxford, 496pp.

550 Campbell, I.H., Griffiths, R.W., 1990. Implications of mantle plume structure for the
551 evolution of flood basalts. Earth and Planetary Science Letters 99, 79-73.

552 Chauvel, C., Goldstein, S.L., Hofmann, A.W., 1995. Hydration and dehydration of oceanic
553 crust controls Pb evolution in the mantle. Chemical Geology 126, 65-75.

554 Chavez Gomez, S., 2001. A catalogue of dykes from aeromagnetic surveys in eastern and
555 southern Africa. ITC publication number 80.

556 Coltice, N., Phillips, B.R., Bertrand, H., Ricard, Y., Rey, P., 2007. Global warming of the
557 mantle at the origin of flood basalts over supercontinents. Geology 35, 391-394.

558 Coltice, N., Bertrand, H., Rey, P., Jourdan, F., Philipps, B.R., Ricard Y., Global warming of
559 the mantle beneath continents back to the Archean; submitted to Gondwana Research.

560 Courtillot, V., Jaupart, C., Manighetti, I. Tapponnier, P., Besse, J., 1999. On causal links
561 between flood basalts and continental breakup. Earth and Planetary Science Letters 166,
562 177-195.

563 Courtillot, V.E., Renne, P. R., 2003. On the ages of flood basalt events. Comptes Rendus
564 Geosciences 335, 113-140.

565 Cox, K.G., MacDonald, R., Hornung, G., 1967. Geochemical and petrogenetic provinces in
566 the Karroo basalts of southern Africa. *American Mineralogist* 52, 1451-1474.

567 Cox, K.G., 1988. The Karoo Province. In: J.D. MacDougall (Ed), *Continental Flood Basalts*.
568 Kluwer, Boston, pp. 239-271.

569 Dalziel, I.W.D., Mosher, S., Gahagan, L.M., 2000. Laurentia-Kalahari collision and the
570 assembly of Rodinia. *The Journal of Geology* 108, 499-513.

571 Duncan, A.R., Erlank, A.J., Marsh, J.S., 1984. Regional geochemistry of the Karoo igneous
572 province. In: A.J. Erlank (Editor), *Petrogenesis of the volcanic rocks of the Karoo*
573 *province*. Geological Society Special Publication of South Africa., pp. 355-388.

574 Elburg, M., Goldberg, A., 2000. Age and geochemistry of Karoo dolerite dykes from
575 northeast Botswana. *Journal of African Earth Sciences* 31, 539-554.

576 Ellam, R.M., Carlson, R.W., Shirley, S.B., 1992. Evidence from R-Os isotopes for plume-
577 lithosphere mixing in Karoo flood basalt genesis. *Nature* 359, 718-721.

578 Eriksson, P.G., Condie, K.C., Van der Westhuizen, W., Van der Merwe, R., De Bruijn, H,
579 Nelson, D.R., Altermanna, W., Catuneanu, O., Bumbya, A.J., Lindsay, J.,
580 Cunningham, M.J., 2002. Late Archaean superplume events: a Kaapvaal-Pilbara
581 perspective. *Journal of Geodynamics* 34, 207-247.

582 Ernst, R.E., Buchan, K.L., 2003. Recognizing mantle plumes in the geological record. *Annual*
583 *Review of Earth and Planetary Sciences* 31, 469-523.

584 Féraud, G., Giannérini, G., Campredon, R., 1987. Dyke swarms as paleostress indicators in
585 areas adjacent to continental collision zones: examples from the European and northwest
586 Arabian plates. In: H.C. Halls, Fahrig, W.F. (Eds), *Mafic dyke swarms*. Geological
587 Association of Canada Special Paper, pp. 273-278.

588 Hanson, R.E., Martin, M.W., Bowring, S.A., Munyanyiwa, H., 1998. U-Pb zircon age for the
589 Umkondo dolerites, eastern Zimbabwe: 1.1 Ga large igneous province in southern Africa-
590 East Antarctica and possible Rodinia correlations. *Geology* 26, 1143-1146.

591 Hanson, R.E., Crowley, J.L., Bowring, S. A., Ramezani, J., Gose, W.A., Dalziel, I.W. D.,
592 Pancake, J. A., Seidel, E. K., Blenkinsop, T. G., Mukwakwami, J., 2004. Coeval large-
593 scale magmatism in the Kalahari and Laurentian cratons during Rodinia assembly.
594 *Science* 304, 1126-1129.

595 Hanson, R.E., Harmer, R.E., Blenkinsop, T.G., Buller, D.S., Dalziel, I.W.D., Gose, W.A.,
596 Hall, R.P., Kampunzu, A.B., Key, R.M., Mukwakwami, J., Munyanyiwa, H., Pancake,
597 J.A., Seidel, E.K., Ward, E.K., 2006. Mesoproterozoic intraplate magmatism in the
598 Kalahari Craton: A review. *Journal of African Earth Sciences* 46, 141-167.

599 Hawkesworth, C., Kelley, S., Turner, S., Le Roex, A., Storey, B., 1999. Mantle processes
600 during Gondwana break-up and dispersal. *Journal of African Earth Sciences* 28, 239-261.

601 Hawkesworth, C.J., Marsh, J.S., Duncan, A.R., Erlank, A.J., Norry, M.J., 1984. The role of
602 continental lithosphere in the generation of the Karoo volcanic rocks: evidence from
603 combined Nd- and Sr-isotope studies. In: A.J. Erlank (Ed), *Petrogenesis of the volcanic
604 rocks of the Karoo province. Geological Society Special Publication of South Africa.*, pp.
605 341-354.

606 Hill, R.I., 1991. Starting plume and continental break-up. *Earth and Planetary Science Letters*
607 104, 398-416.

608 Iacumin, M., De Min, A., Piccirillo, E. M., Bellieni, G., 2003. Source mantle heterogeneity
609 and its role in the genesis of Late Archaean-Proterozoic (2.7-1.0 Ga) and Mesozoic (200
610 and 130 Ma) tholeiitic magmatism in the South American Platform. *Earth-Science
611 Reviews* 62, 365-397.

612 Ikingura, J.R., Bell, K., Watkinson, D.H., Van Straaten, P., 1990. Geochronology and
613 chemical evolution of granitic rocks, NE Kibaran (Karagwe-Ankolean) belt, NW
614 Tanzania. In: G. Rocci, Deschamps, M. (Ed), *Recent Data in African Earth Sciences.*
615 International Center for Training and Exchanges in the Geosciences Occasional
616 Publication, pp. 97-99.

617 Jonhson, S.P., Oliver, G.J.H., 2000. Mesoproterozoic oceanic subduction, island arc
618 formation and the initiation of back-arc spreading in the Kibaran Belt of central, southern
619 Africa: evidence from the Ophiolite Terrane, Chewore Inliers, northern Zimbabwe.
620 *Precambrian Research* 103, 2000.

621 Jourdan, F., Marzoli, A., Bertrand, H., Cosca, M., Fontignie., D., 2003. The northernmost
622 CAMP: Ar/Ar age, petrology and Sr-Nd-Pb isotope geochemistry of the Kerforne dyke,
623 Brittany, France. In: W. Hames, J.G. McHone, C. Rupel, P.R. Renne (Ed), *The Central
624 Atlantic Magmatic Province. A.G.U. Monograph*, pp. 209-226.

625 Jourdan, F., Féraud, G., Bertrand, H., Kampunzu, A.B., Tshoso, G., Le Gall, B., Tiercelin,
626 J.J., Capiez P., 2004. The Karoo triple junction questioned: evidence from $^{40}\text{Ar}/^{39}\text{Ar}$
627 Jurassic and Proterozoic ages and geochemistry of the Okavango dyke swarm (Botswana).
628 *Earth and Planetary Sciences Letters* 222, 989-1006.

629 Jourdan, F., Renne, P.R., Mundil, R., 2005. $^{40}\text{Ar}/^{39}\text{Ar}$ and U/Pb Ages and geochemistry of the
630 Benton Range Dike Swarm, SE California: New Evidence for an “Independence” Poly-
631 phased Dike Swarm, in: *Geophysical research abstract, AGU fall meeting*

632 Jourdan, F., Féraud, G., Bertrand, H., Watkeys, M.K., Kampunzu, A.B., Le Gall B., 2006.
633 Basement control on dyke distribution in Large Igneous Provinces: case study of the
634 Karoo triple junction, *Earth and Planetary Science Letters* 241, 307-322.

635 Jourdan F., Bertrand, H., Sharer, U., Blichert-Toft, J., Féraud, G., Kampunzu, A.B., Le Gall,
636 B., Watkeys, M.K., 2007. Major and Trace Element and Sr, Nd, Hf, and Pb Isotope
637 Compositions of the Karoo Large Igneous Province, Botswana-Zimbabwe: Lithosphere vs
638 Mantle Plume Contribution. *Journal of Petrology* 48, 1043-1077

639 Kampunzu, A.B., Akanyang, P., Mapeo, R.B.M., Modie, B.N., Wendorff, M., 1998.
640 Geochemistry and tectonic significance of the Mesoproterozoic Kgwebe metavolcanic
641 rocks in northwest Botswana: implications for the evolution of the Kibaran Namaqua-
642 Natal belt. *Geological Magazine* 135, 669-683.

643 Kampunzu, A.B., Armstrong, R.A., Modisi, M.P., Mapeo, R.B.M., 2000. Ion microprobe U-
644 Pb ages on detrital zircon grains from the Ghanzi Group: implication for the identification
645 of Kibaran-age crust in northern Botswana. *Journal of African Earth Sciences* 30, 579-
646 587.

647 Key, R.M., Ayres, N., 2000. The 1998 edition of the National Geological Map of Botswana.
648 *Journal of African Earth Sciences* 30, 427-451.

649 Kokonyangi, J., Armstong, R., Kampunzu, A.B., Yoshida, M., Okudaira, T., 2004. U-Pb
650 zircon geochronology and petrology of granitoids from Mitwaba (Katanga, Congo):
651 implications for the evolution of the Mesoproterozoic Kibaran belt. *Precambrian Research*
652 132, 79-106.

653 Kruger, F.J., Geringer, G.J., Havenga, A.T., 2000. The geology, Petrology, geochronology
654 and source region character of the layered gabbro-noritic Orangekom Complex in the
655 Kibaran Namaqua mobile belt, South Africa. *Journal of African Earth Sciences* 30, 667-
656 687.

657 Le Bas, M.J., Le Maitre, R.W., Streickeisen, A., Zanettin, B., 1986. A chemical classification
658 of volcanic rocks based on the total alkali silica diagram. *Journal of Petrology* 27, 745-
659 750.

660 Le Gall, B., Tshoso, G., Jourdan, F., Féraud, G., Bertrand, H., Tiercelin, J.J., Kampunzu, A.B.
661 Modisi, M.P., Dymant, M., Maia, J., 2002. $^{40}\text{Ar}/^{39}\text{Ar}$ geochronology and structural data
662 from the giant Okavango and related mafic dyke swarms, Karoo igneous province,
663 Botswana. *Earth and Planetary Science Letters* 202, 595-606.

664 Le Gall B., Tshoso, G., Dymant, J. Kampunzu, A. B., Jourdan, F., Féraud, G., Bertrand, H., &
665 Aubourg, C., 2005. The Okavango giant mafic dyke swarm (NE Botswana) and its

666 structural significance within the Karoo Large Igneous Province. *Journal of Structural*
667 *Geology* 27, 2234-2255.

668 Luttinen, A.V., Furnes, H., 2000. Flood basalts of Vestfjella: Jurassic magmatism across an
669 Archaean-Proterozoic Lithospheric Boundary in Droning Maud Land, Antarctica. *Journal*
670 *of Petrology* 41, 1271-1305.

671 McKenzie, D., O'Nions, R.K., 1991. Partial melt distribution from inversion of rare earth
672 element concentrations. *Journal of Petrology* 32, 1021-1091.

673 Molzahn, M., Reisberg, L., 1996. Os, Sr, Nd, Pb, O isotope and trace element data from the
674 Ferrar flood basalts, Antarctica: evidence for an enriched subcontinental lithospheric
675 source. *Earth and Planetary Science Letters* 144, 529-545.

676 Morgan, W.J., 1981. Hot spot tracks and the opening of the Atlantic and Indian Oceans. In: C.
677 Emiliani (Editor), *The Sea*, 7. Wiley Interscience, New York, pp. 443-487.

678 Munyanyiwa, H., 1999. Geochemical study of the Umkondo dolerites and lavas in
679 Chimanmani and Chipige Districts (eastern Zimbabwe) and their regional implications.
680 *Journal of African Earth Sciences* 28, 349-365.

681 Murphy, J.B., Hynes, A.J., 1986. Contrasting secondary mobility of Ti, P, Zr, Nb and Y in
682 two metabasaltic suites in the Appalachians. *Canadian Journal of Earth Sciences* 23, 1138-
683 1144.

684 Nomade, S., Pouclet, A., Chen, Y., 2002. The French Guyana dolerite dykes: geochemical
685 evidence of three populations and new data for the Jurassic Central Atlantic magmatic
686 province. *Journal of Geodynamics* 34, 595-614.

687 Peng, Z.X., Mahoney, J.J., 1995. Drillhole lavas from the northwestern Deccan Traps, and the
688 evolution of Réunion hotspot mantle. *Earth and Planetary Science Letters* 134, 169-185.

689 Pik, R., Deniel, C., Coulon, C., Yirgu, G., Marty, B., 1999. Isotopic and trace element
690 signatures of Ethiopian flood basalts: Evidence for plume-lithosphere. *Geochimica and*
691 *Cosmochimica Acta* 15, 2263-2279.

692 Reeves, C., 2000. The geophysical mapping of Mesozoic dyke swarms in southern Africa and
693 their origin in the disruption of Gondwana. *Journal of African Earth Sciences* 30, 499-513.

694 Reimold, W.U., Pybus, G.Q.J., Kruger, F.J., Layer, P.W., Koeberl, C., 2000. Anna's Rust
695 Sheet and related gabbroic intrusion in the Vredefort Dome - Kibaran magmatic event on
696 the Kaapvaal Craton and beyond? *Journal of African Earth Sciences* 31, 499-521.

697 Saunders, A.D., Storey, M., Kent, R.W., Norry, M.J., 1992. Consequences of plume-
698 lithosphere interactions. In: B.C. Storey, Alabaster, T., Pankhurst, R.J. (Ed), *Magmatism*

- 699 and the causes of continental break-up. Geological Society of London Special Publication,
700 pp. 41-60.
- 701 Schwartz, M.O., Kwok, Y.Y., Davis, D.W., Akanyang, P., 1996. Geology, geochronology and
702 regional correlation of the Ghanzi Ridge, Botswana. South African Journal of Geology 99,
703 245-250.
- 704 Shaw, D.M. (1967). Trace element fractionation during anatexis. *Geochemica, Cosmochimica*
705 *Acta* 34, 237-234.
- 706 Singletary, S.J., Hanson, R.E., Martin, M.K., Crowley, J.L., Bowring, S.A., Key, R.M.,
707 Ramokate, L.V., Dreng, B.B., Krol, M.A., 2003. Geochronology of basement rocks in the
708 Kalahari Desert, Botswana, and implications for regional Proterozoic tectonics.
709 *Precambrian Research* 121, 47-71.
- 710 Sun, S.S., McDonough, W.F., 1989. Chemical and isotopic systematics of oceanic basalts:
711 implication for mantle composition and processes. In: A.D. Saunders, Norry, M.J.
712 (Editor), *Magmatism in the ocean basin*. Blackwell, Oxford.
- 713 Sweeney, R.J., Duncan, A.R., Erlank, A.J., 1994. Geochemistry and petrogenesis of Central
714 Lebombo basalts from the Karoo Igneous Province. *Journal of Petrology* 35, 95-125.
- 715 Sweeney, R.J., Watkeys, M.K., 1990. A possible link between Mesozoic lithospheric
716 architecture and Gondwana flood basalts. *Journal of African Earth Sciences* 10, 707-716.
- 717 Tshoso, G., Dymant, J., Aubourg, C., Legall, B., Tiercelin, J.J., Féraud, G., Bertrand, H.,
718 Jourdan, F., Kampunzu, A.B., 2002. Magnetic Investigations on the Okavango Giant
719 Dyke Swarm (N Botswana). *E.G.S. XXVII Geophysical Research Abstracts Nice*, pp. 78.
- 720 Ward S.E., Hall, R.P., Hughes, D.J., 2000. Guruve and Mutare dykes: preliminary
721 geochemical indication for complex Mesoproterozoic mafic magmatic systems in
722 Zimbabwe. *Journal of African Earth Sciences* 30, 689-701.
- 723 White, R.S., McKenzie, D.P., 1989. Magmatism at rift zones: the generation of volcanic
724 continental margins and flood basalts. *Journal of Geophysical Research* 94, 7685-7729.
- 725 Wilson, M., 1997. Thermal evolution of the Central Atlantic margins: continental break-up
726 above a Mesozoic super-plume. *Journal of Geological Society of London* 154, 491-495.

727
728

729 **Figure and table captions**

730
731

732 Figure 1: A) Distribution of the Karoo magmatism and major related dyke swarms ([modified](#)
733 [after Jourdan et al., 2004 and references inside](#)). ODS: Okavango dyke swarm; PODS:
734 Proterozoic Okavango dyke swarm; ORDS: Olifants River dyke swarm; SBDS: South
735 Botswana dyke swarm; SLDS: Sabi-Limpopo dyke swarm; SleDS: South Lesotho dyke
736 swarm; SMDS: South Malawi dyke swarm; RRDS: Rooi Rand dyke swarm; LDS: Lebombo
737 dyke swarm (undated, intruding Karoo lava-pile); GDS: Gap dyke swarm (undated, intruding
738 Karoo sediments). Dotted line corresponds to Botswana border. Thick dashed line
739 corresponds to the hypothesized limit of the Umkondo large igneous province (UIP; cf. [Fig.](#)
740 [10](#)). B) Sketch map of northeastern Botswana showing the N110° oriented ODS-PODS and
741 location of Bot0003 samples. Lava flows exposures are indicated. C) 100 km-long section
742 along the Shashe River, with the location of Proterozoic samples only ([modified after Jourdan](#)
743 [et al., 2004](#)).

744

745 Figure 2: Selected major elements vs. Mg# [100 x atomic ratio of Mg/(Mg+Fe²⁺) with
746 Fe₂O₃/FeO normalized to 0.15]. Low-Ti Karoo basalts ([Jourdan et al., 2007](#)) and Umkondo
747 igneous rocks ([see text for references](#)) were indicated for comparison (see discussion). The
748 low-Mg# group is surrounded by dashed curve.

749

750 Figure 3: Selected trace elements vs. Mg#. Caption as in Figure 2.

751

752 Figure 4. Primitive mantle normalized ([Sun and McDonough, 1989](#)) incompatible trace
753 elements patterns for (A) PODS and related sills with the low-Mg# group indicated by dashed
754 curves (B) Umkondo igneous province (UIP; see text for references) and (3). Karoo low-Ti
755 basalts and sills ([Jourdan et al., 2007](#)).

756

757 Figure 5. Chondrite-normalized ([Boynton, 1984](#)) REE compositions for (A) PODS and
758 related sills with the low-Mg# group indicated by dashed curves, (B) Umkondo igneous
759 province (UIP; see text for references) and (C) Karoo low-Ti basalts and sills ([Jourdan et al.,](#)
760 [2007](#)).

761

762 Figure 6. (Sm/Yb)_n vs. (La/Sm)_n and (La/Yb)_n vs. (Eu/Yb)_n plots for the PODS and related
763 sills, Karoo low- and high-Ti basalts and sills and UIP. Non-modal batch melting modeling
764 curves of lherzolite mantle source are indicated. Partition coefficients are from [McKenzie and](#)
765 [O'Nions \(1991\)](#). The ticks on the curves correspond to melting rates. Melting curve of a

766 spinel-bearing lherzolite source (modal composition 55% olivine, 15% orthopyroxene, 28%
767 clinopyroxene and 2% spinel). Melting mode: 20% olivine, 20% orthopyroxene, 55%
768 clinopyroxene, 5% spinel. PODS source preferred composition: La=1.80, Sm=0.75 Eu=0.23
769 and Yb=0.55 (black dashed curve). Karoo best-fit source composition: La=1.10, Sm=0.67
770 Eu=0.24 and Yb=0.55 (gray plain curve). The gray dashed-dotted curve represents the
771 calculated garnet-bearing mantle source as proposed in [Jourdan et al. \(2007\)](#), indicated for
772 comparison.

773

774 Figure 7. Al₂O₃ and CaO vs. Mg# for the basaltic samples and MELTS ([Ghiorso and Sack,](#)
775 [1995](#)) fractional crystallization modeling curves. Calculation parameters: Pressure and H₂O
776 content are varying between 0.5 Kbars and 5 Kbars and 0% and 2% respectively. fO₂=QFM
777 (quartz-fayalite-magnetite). Starting composition: rock Bot0003 (Mg# = 66); note that adding
778 H₂O in the starting rock composition shift its SiO₂ composition because the total composition
779 is normalized to 100%.

780

781 Figure 8. La/Ba vs. La/Nb plot for the PODS, UIP and Karoo low-Ti basalts and sills. Fields
782 reported as in [Saunders et al. \(1992\)](#).

783

784 Figure 9. Ti/Y vs. Zr/Y plot for the PODS, UIP and Karoo low-Ti basalts and sills. Fields
785 reported from [Brewer et al. \(1992\)](#). The low-Mg# group is indicated by a dashed curve.

786

787 Figure 10. Distribution of the 1.1 Ga Umkondo large igneous province ([after Hanson et al.,](#)
788 [1988 and 2004](#)). The locations of the samples used for geochemical comparison are quoted in
789 bold. PODS black dashed line indicates possible extension of the dyke swarm by comparison
790 with the ODS. Thin dotted line: Botswana border. Thick dashed line: schematic “Kibaran-
791 aged” belts represented with basement fabrics.

792

793 Table 1. Major (wt%) and trace and RE elements (ppm) analyses for the PODS and related
794 sills rocks. LOI: loss on ignition. Most trace elements of most samples were determined by
795 ICPMS except those quoted in italic, measured by XRF.

796

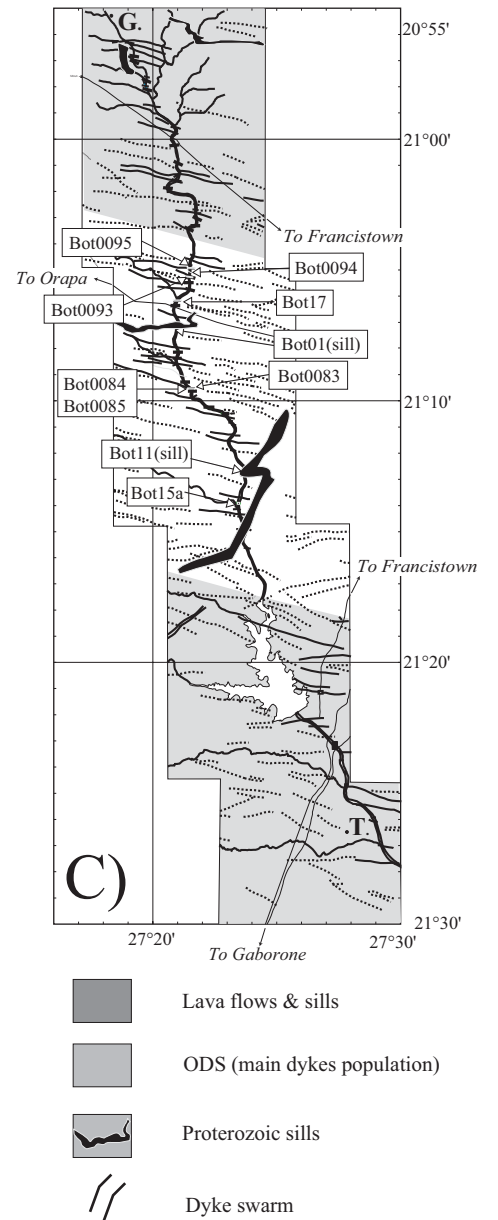
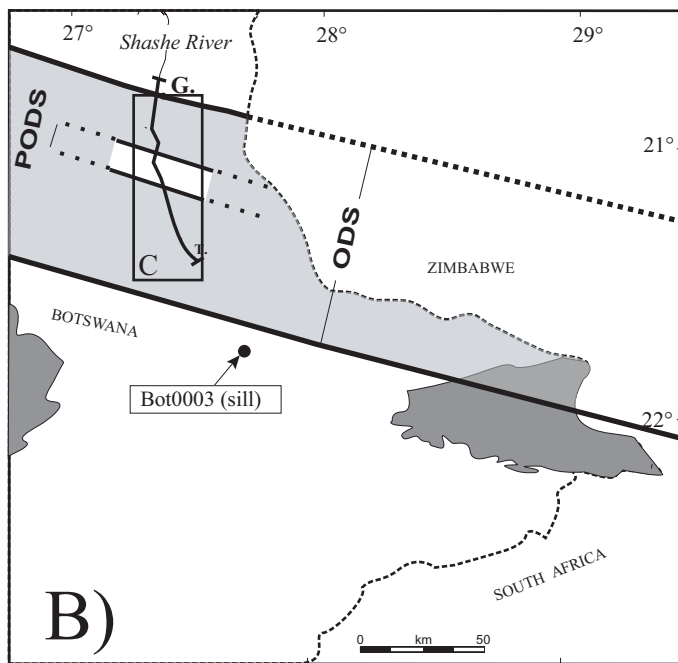
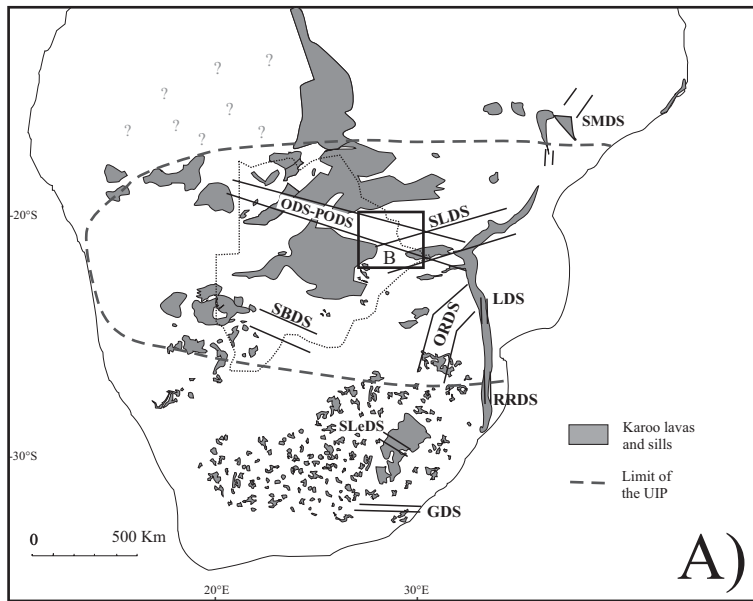


Figure 1

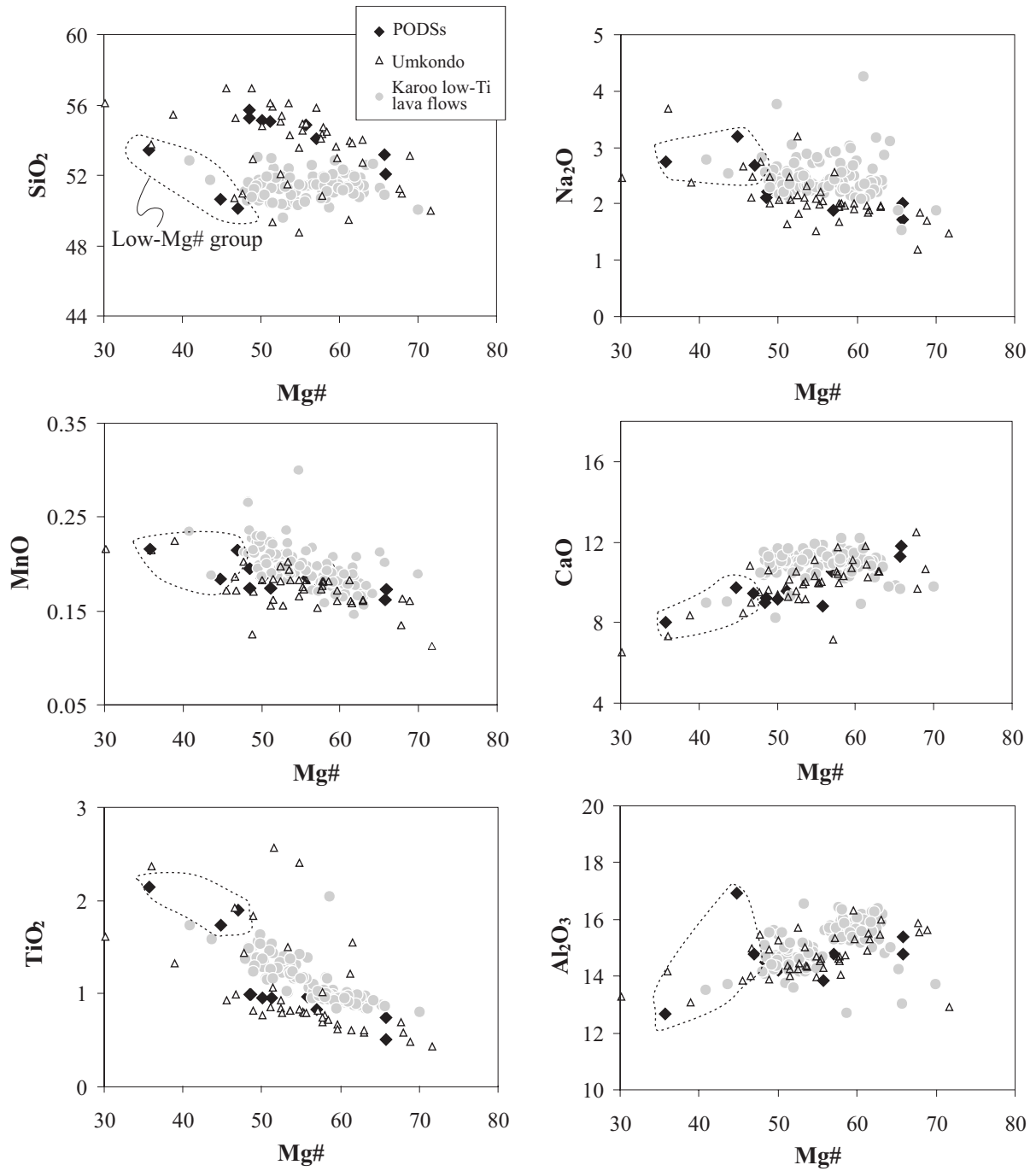


Figure 2

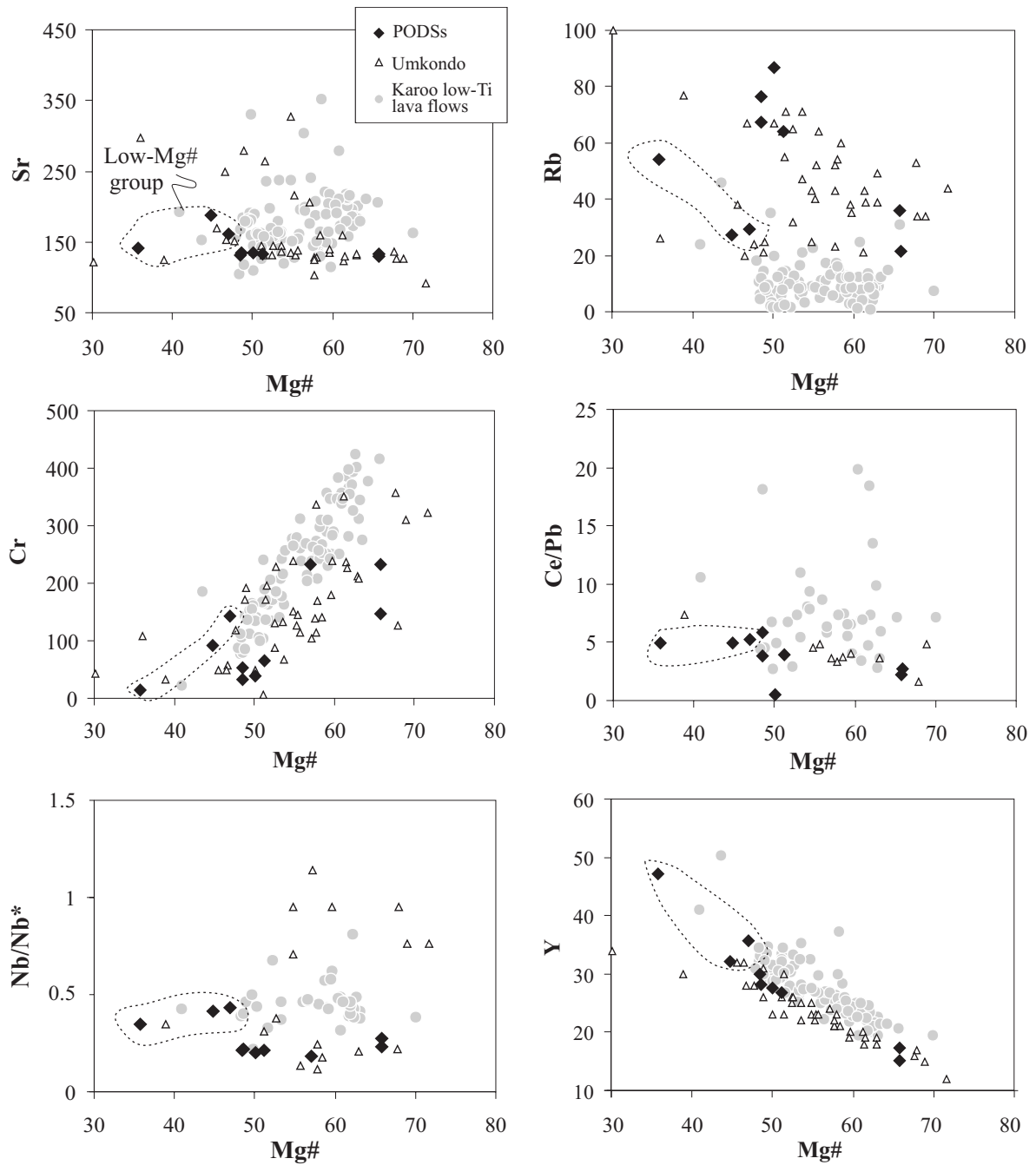


Figure 3

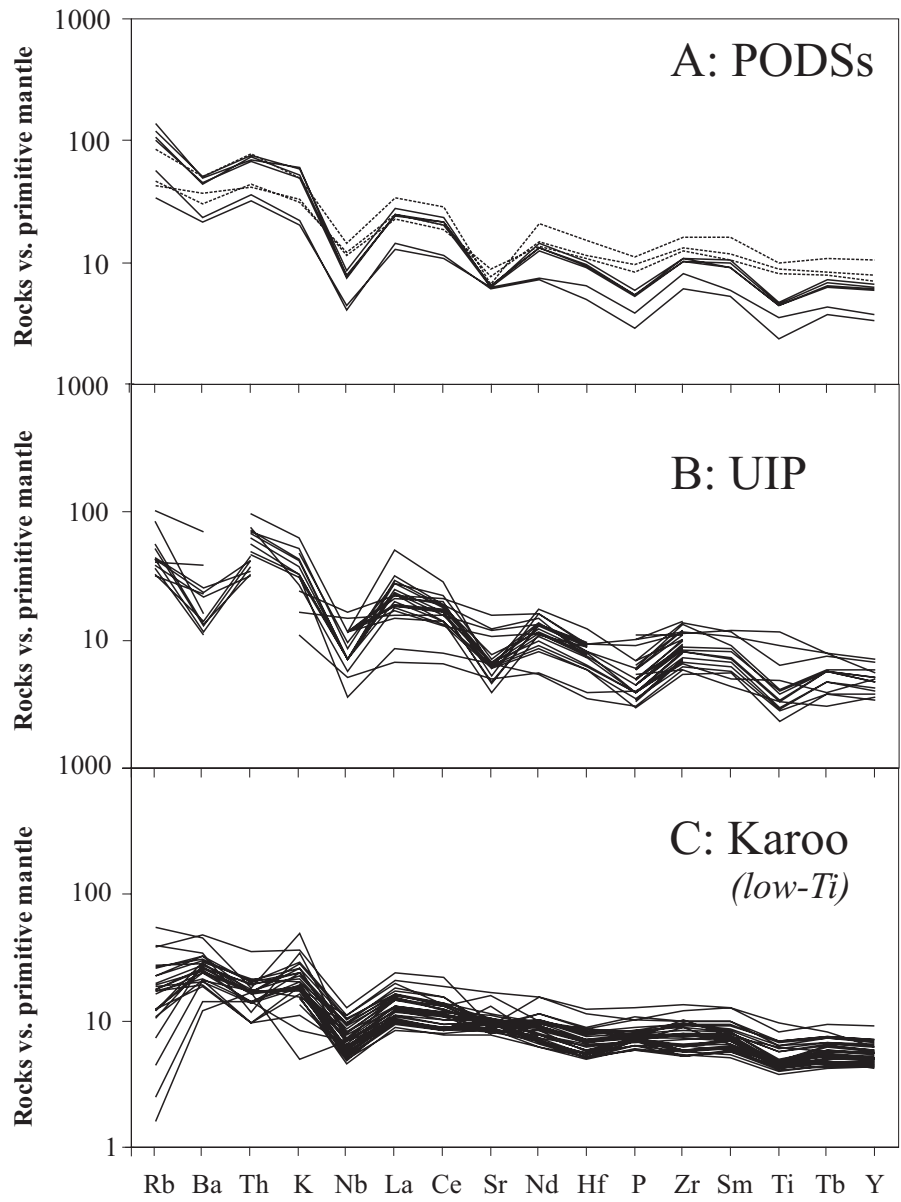


Figure 4

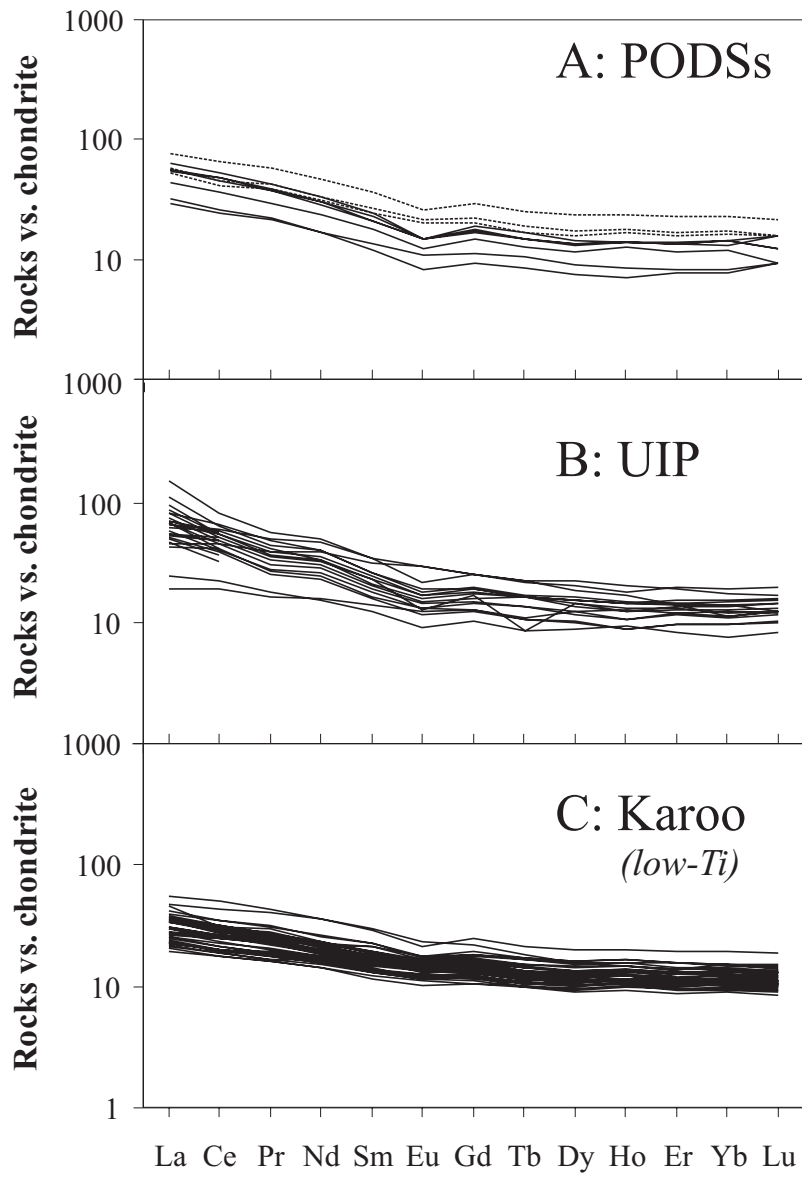


Figure 5

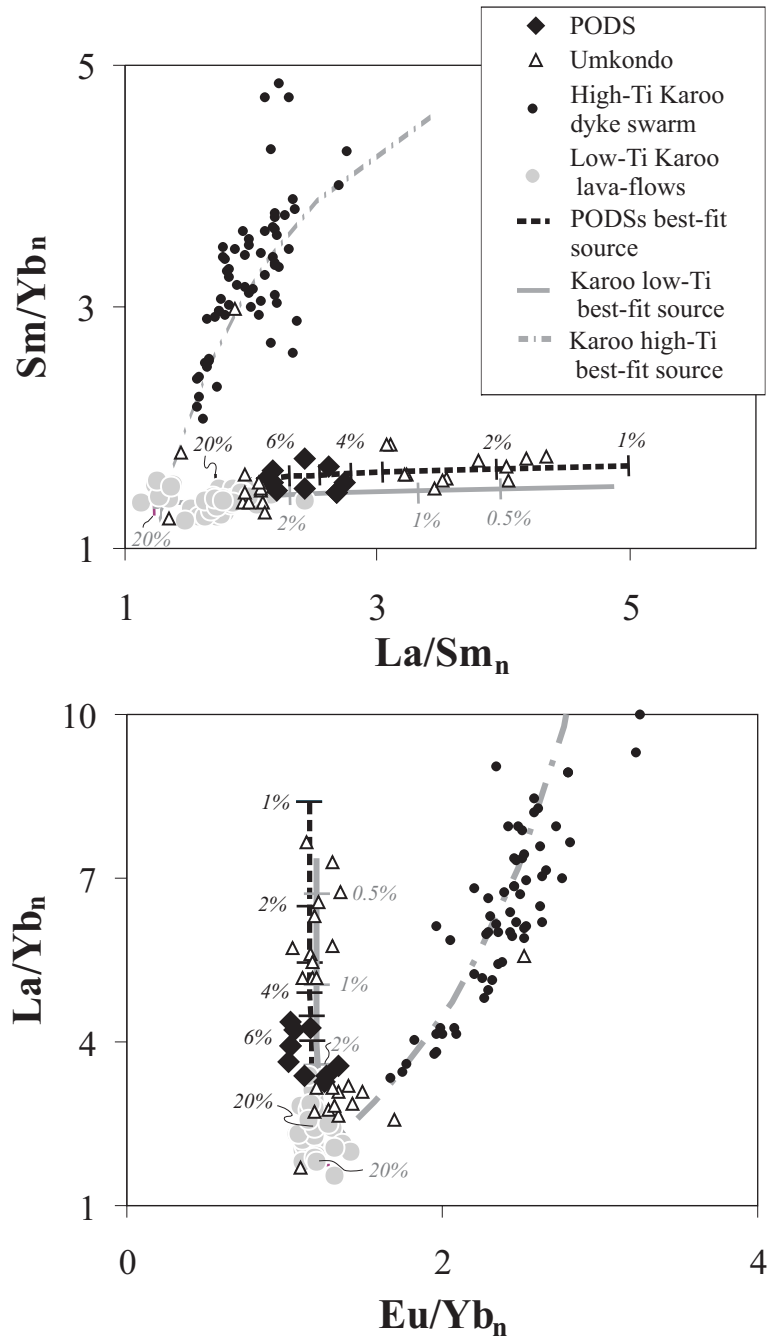


Figure 6

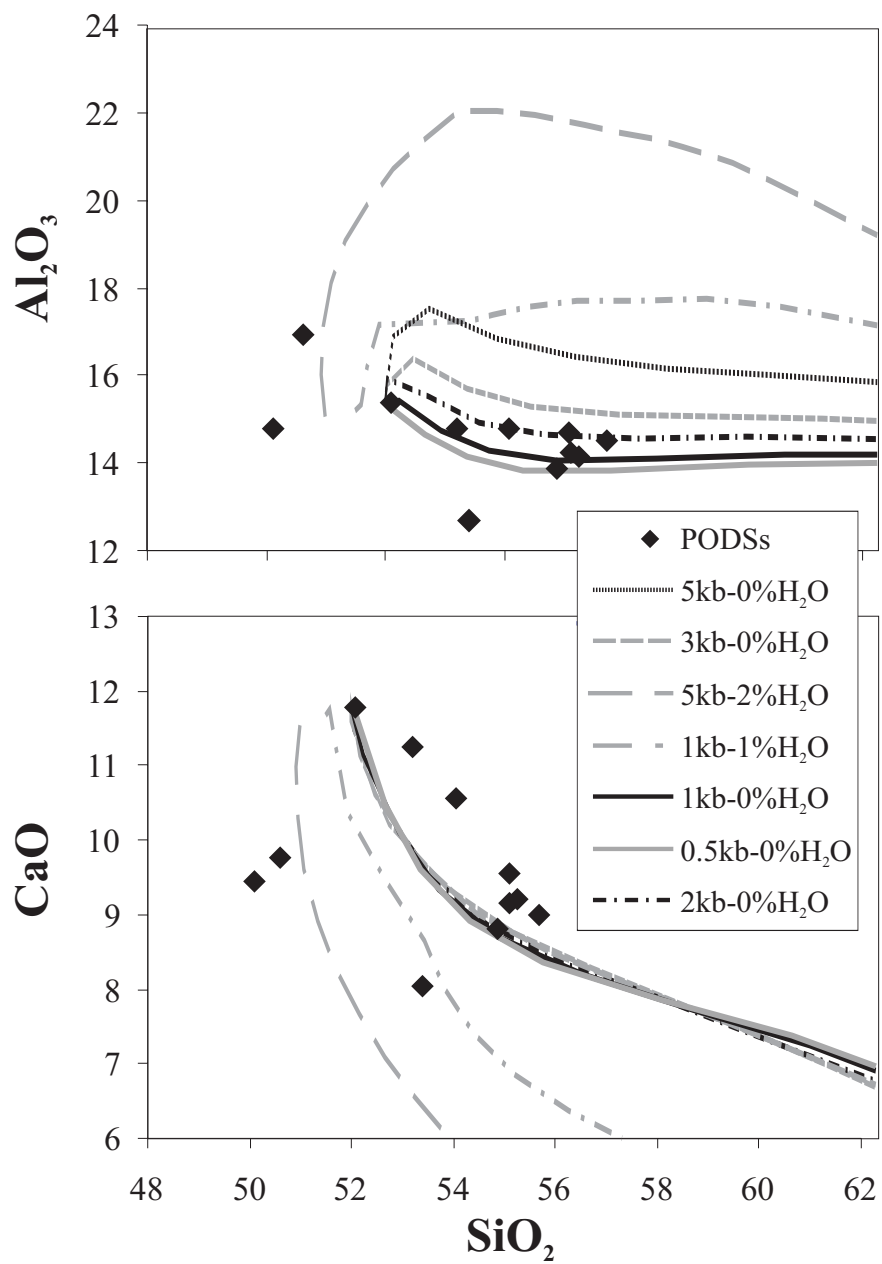


Figure 7: Jourdan et al.

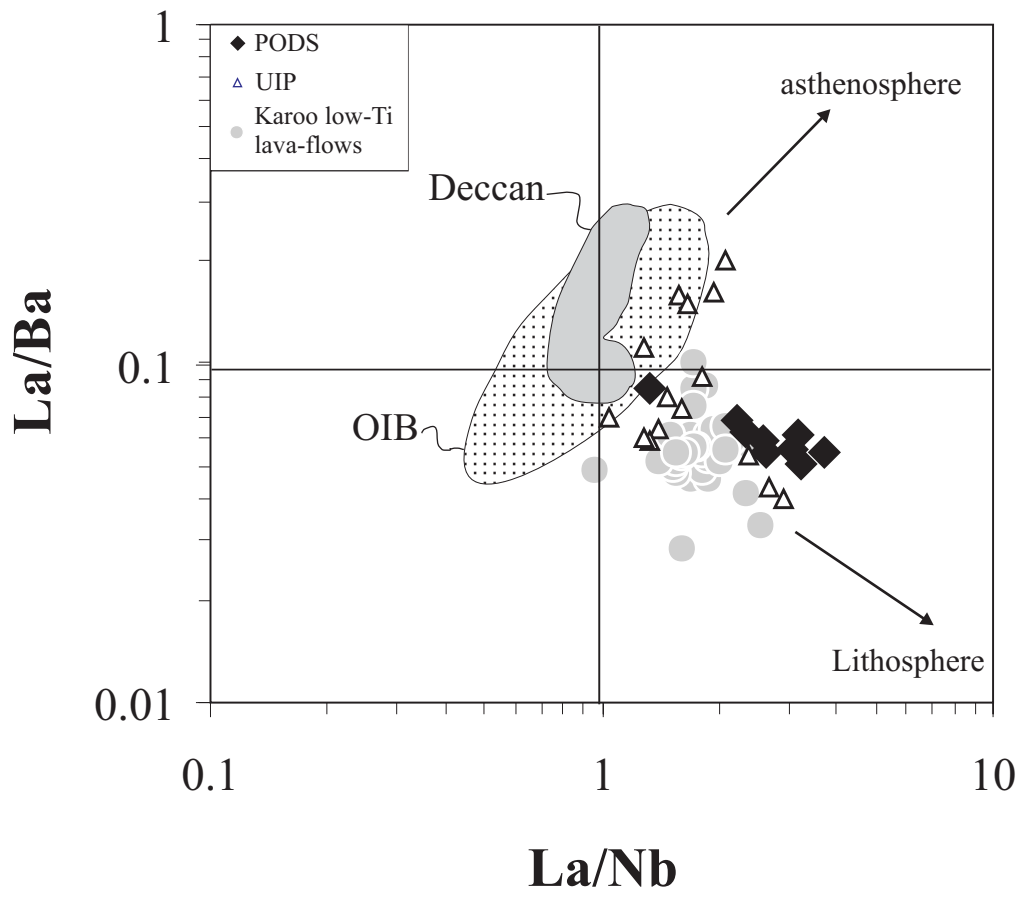


Figure 8

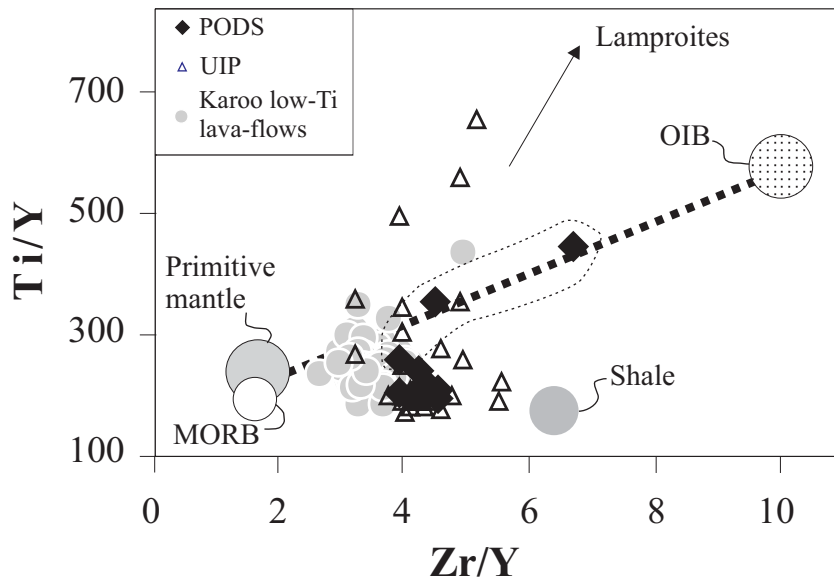


Figure 9

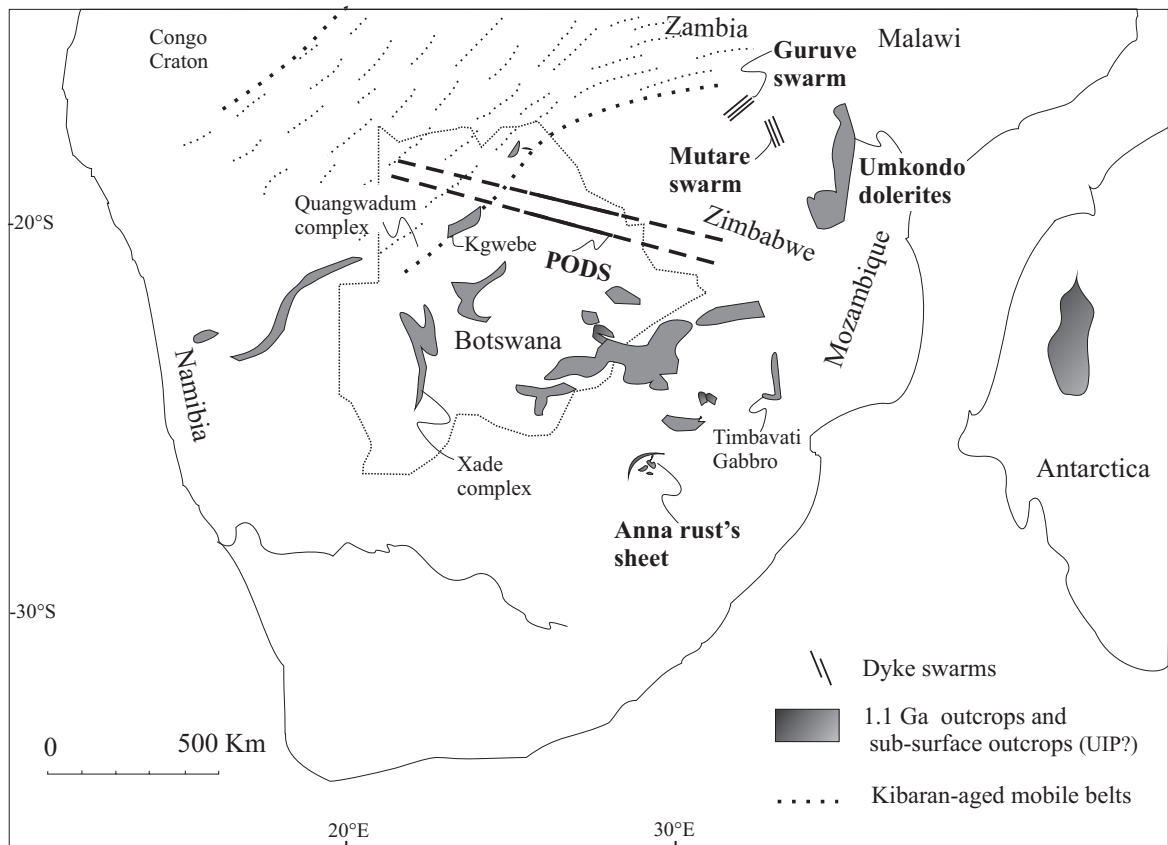


Figure 10

Type Sample	Sill Bot01	Sill Bot11	Dyke Bot15A	Dyke Bot17	Dyke Bot0083	Dyke Bot0084	Dyke Bot0085	Dyke Bot0093	Dyke Bot0094	Dyke Bot0095	Sill Bot0003
<i>Major elements (wt%)</i>											
SiO ₂	52.06	49.49	48.93	52.39	53.31	54.32	53.95	53.42	53.70	53.65	51.09
Al ₂ O ₃	12.36	16.56	14.43	14.54	14.59	14.13	14.37	13.49	13.75	13.85	15.08
Fe ₂ O ₃	16.36	12.89	15.09	9.95	11.11	11.76	11.54	11.43	12.19	11.96	9.92
MgO	3.91	4.49	5.74	8.20	6.32	4.75	5.20	6.19	4.94	5.15	8.20
CaO	7.84	9.54	9.23	11.09	10.42	8.78	9.36	8.58	8.95	8.92	11.57
Na ₂ O	2.67	3.13	2.62	1.98	1.86	2.06	2.06	2.29	2.15	2.10	1.68
K ₂ O	1.39	0.92	0.87	0.63	1.04	1.65	1.39	1.87	1.48	1.69	0.58
TiO ₂	2.09	1.70	1.85	0.50	0.82	0.97	0.94	0.94	0.96	0.93	0.73
P ₂ O ₅	0.23	0.17	0.20	0.06	0.09	0.12	0.11	0.09	0.11	0.11	0.08
MnO	0.21	0.18	0.21	0.16	0.17	0.17	0.17	0.18	0.19	0.18	0.17
LOI	0.51	0.89	0.62	0.93	0.51	1.14	1.17	0.88	1.35	1.42	0.83
H ₂ O	0.18	-	0.18	-	0.13	0.17	0.09	0.90	0.18	0.21	-
TOTAL	99.81	99.96	99.97	100.43	100.37	100.02	100.35	100.26	99.95	100.17	99.93
Mg#	35.77	44.81	46.99	65.76	57.00	48.49	51.22	55.79	48.57	50.09	65.83
<i>Trace elements (ppm)</i>											
Rb	54	27	29	36	47	77	64	99	67	87	21
Ba	351	261	215	163	219	351	320	473	309	343	152
Th	6.48	3.50	3.67	3.06	-	6.38	5.62	-	6.19	5.91	2.72
Nb	10.24	8.12	8.61	2.92	3.40	6.10	5.33	4.30	5.65	5.42	3.20
Sr	142	188	161	129	118	131	132	197	135	134	132
Hf	5.27	3.76	4.05	1.72	-	3.61	3.19	-	3.33	3.30	2.26
Zr	182	139	147	68	95	122	113	99	114	122	91
Y	47.2	32.1	35.7	15.2	24.2	30.1	26.8	20.9	28.2	27.5	17.2
Pb	10.59	6.79	7.04	9.59	-	7.36	9.37	-	10.12	79.46	7.23
Ta	0.79	0.59	0.61	<0.5	-	<0.5	<0.5	-	<0.5	<0.5	<0.5
U	1.30	0.71	0.64	0.77	-	1.24	1.08	-	1.09	1.09	0.56
Sc	33	33	31	31	32	36	31	26	34	33	30
V	406	336	328	208	239	247	249	227	255	252	206
Cr	7	87	100	222	109	50	69	185	32	28	216
Co	49	37	38	47	50	45	45	47	47	47	44
Ni	52	48	55	128	97	76	83	69	70	78	104
La	24.11	16.32	15.09	17.78	10.09	-	19.51	17.34	17.22	17.33	9.19
Ce	52.50	33.61	32.45	37.22	21.06	-	42.92	36.83	39.20	38.88	19.59
Pr	7.14	4.70	4.48	5.10	2.69	-	5.16	4.60	4.66	4.60	2.63
Nd	28.16	18.69	18.02	20.21	9.98	-	19.77	17.03	18.11	18.03	10.03
Sm	7.10	4.71	4.51	5.23	2.31	-	4.68	4.07	4.36	4.05	2.65
Eu	1.85	1.48	1.36	1.57	0.59	-	1.11	1.09	1.08	1.08	0.77
Gd	7.46	5.27	5.00	5.82	2.44	-	4.88	4.35	4.65	4.51	2.90
Tb	1.18	0.85	0.80	0.89	0.40	-	0.77	0.68	0.73	0.69	0.47
Dy	7.59	5.14	4.81	5.59	2.36	-	4.57	4.21	4.40	4.33	2.85
Ho	1.69	1.22	1.13	1.28	0.54	-	1.03	0.98	1.03	1.03	0.63
Er	4.80	3.28	3.19	3.53	1.59	-	2.94	2.80	2.77	2.78	1.73
Yb	4.85	3.35	3.16	3.58	1.64	-	3.04	2.97	2.72	3.01	1.70
Lu	0.73	0.50	0.47	0.53	0.25	-	0.47	0.42	0.45	0.44	0.27

Table 1: Jourdan et al.